

# Testing neutrino oscillations plus decay with neutrino telescopes

---

**Michele Maltoni**

*Departamento de Física Teórica & Instituto de Física Teórica UAM/CSIC, Facultad de Ciencias C-XI, Universidad Autónoma de Madrid, Cantoblanco, E-28049 Madrid, Spain*  
*E-mail: michele.maltoni@uam.es*

**Walter Winter**

*Institut für theoretische Physik und Astrophysik, Universität Würzburg,  
D-97074 Würzburg, Germany*  
*E-mail: winter@physik.uni-wuerzburg.de*

**ABSTRACT:** We discuss the interplay of neutrino oscillation and decay properties at neutrino telescopes. Motivated by recent unparticle scenarios, which open the possibility of new neutrino decay modes over astrophysical distances, we perform a complete classification of possible decay schemes, and we illustrate how different scenarios can be identified. Moreover, we show that the sensitivity of neutrino telescopes to standard neutrino properties, such as the mass hierarchy or  $\delta_{CP}$ , is greatly enhanced in specific decay scenarios. In particular we discuss the impact of an astrophysical neutrino detection on terrestrial experiments, such as on the mass hierarchy measurement at  $NO\nu A$ . For example, we find that the scenario where only  $\nu_1$  is stable can be uniquely identified against all the other decay schemes, and that in this case CP violation can be established (for large  $\theta_{13}$ ) by the combination of Double Chooz with the track-to-shower ratio at a neutrino telescope, even if the flavor composition at the source is unknown. Our statements are based on a complete analysis of all the present solar, atmospheric, reactor and accelerator neutrino data, as well as on realistic simulation of future terrestrial neutrino oscillation experiments.

**KEYWORDS:** neutrino oscillations, neutrino decay, neutrino telescopes.

---

## Contents

<b>1. Introduction</b>	<b>1</b>
<b>2. Considered physics scenarios</b>	<b>3</b>
<b>3. Physics scenario identification</b>	<b>7</b>
<b>4. Neutrino mass hierarchy</b>	<b>11</b>
<b>5. Generalized source or diffuse flux</b>	<b>14</b>
<b>6. Glashow resonance process as a third observable?</b>	<b>17</b>
<b>7. Synergies with terrestrial neutrino oscillation experiments</b>	<b>18</b>
7.1 Can Double Chooz plus neutrino telescope measure $\delta_{\text{CP}}$ ?	18
7.2 Octant determination terrestrial experiments plus neutrino telescope	19
7.3 Mass hierarchy determination with $\text{NO}\nu\text{A}$ plus astrophysical	20
<b>8. Summary and conclusions</b>	<b>21</b>
<b>A. Statistical method and simulation</b>	<b>22</b>
<b>B. Movies</b>	<b>24</b>

---

## 1. Introduction

Neutrino telescopes [1, 2, 3, 4] are sensitive to neutrinos with an average energy and traveled distance many orders of magnitude larger than present neutrino experiments, and provide therefore a completely new window on both standard and non-standard neutrino properties. Apart from “conventional” parameters, such as neutrino masses and mixing angles, a very prominent example of such properties is the neutrino lifetime. Phenomenologically, from the observation of neutrinos from supernova 1987A, we know that at least one neutrino mass eigenstate must be stable over galactic distances. More stringent and explicit bounds can be derived from different observations when specific decay models are assumed (see, *e.g.*, Refs. [5, 6, 7] for an overview). For example, solar neutrinos strongly limit the possibility of radiative decays [8], while for Majoron decays [9, 10] explicit bounds can be obtained from neutrinoless double-beta decay and supernovae [11]. Purely phenomenological (*i.e.*, model-independent) bounds are, however, much weaker, leaving enough parameter space for the decay of any mass eigenstate over extragalactic distances [12, 13, 14]. In view of the recently proposed unparticle models, which may lead to new mechanisms of neutrino

decay [15, 16, 17, 18], we do not assume any specific decay model, but study the most general case. Note that neutrino telescopes may also probe different kinds of new physics (see, *e.g.*, Refs. [7, 19, 20]), which we do not discuss in this work.

In addition to decay properties, the propagation from the neutrino source to the detector is described by the neutrino mixing parameters through averaged neutrino oscillations. If the neutrino telescope has some flavor identification capability, this dependence can be used to extract information on the decay [21, 18] and oscillation [22, 23, 24, 25, 26, 27, 28, 29, 30, 31] parameters, in a way which might be synergistic to terrestrial measurements. For example, reactor neutrino experiments in combination with astrophysical observations might provide hints on  $\delta_{\text{CP}}$  well before superbeams, by measuring the CP-even part of the oscillation probabilities [26, 27]. In addition, the sensitivity to the oscillation parameters can be enhanced in some decay scenarios [32]. In this study, we discuss the identification of the various neutrino properties in scenarios with both neutrino oscillations and decay. Since uncertainties in the oscillation parameters [33] and flavor composition at the source [34] may limit such measurements, we carefully include these aspects in our study.

**Astrophysical sources and flavor composition.** The existence of astrophysical neutrinos is not yet proven, but the detection of very high energy cosmic rays points towards cosmic accelerators which are expected to produce in addition high energy neutrinos. There are many potential candidates for neutrino sources, such as gamma ray bursts, active galactic nuclei or starburst galaxies, the latter being unaffected by the Waxmann-Bahcall bound [35]. Astrophysical neutrinos are normally assumed to originate from pion decays, with a flavor ratio at the source of  $(f_e, f_\mu, f_\tau) \simeq (1/3, 2/3, 0)$  arising from the decays of both primary pions and secondary muons (“pion beam source”); here  $f_\alpha$  is the fraction of flavor  $\nu_\alpha$  (neutrinos and antineutrinos combined), so that  $f_e + f_\mu + f_\tau = 1$ . However, it was pointed out in Ref. [36] that such sources may become opaque to muons at higher energies, in which case the flavor ratio at the source changes to  $(f_e, f_\mu, f_\tau) \simeq (0, 1, 0)$  (“muon damped source”). Therefore, one can expect a smooth transition from one type of source to the other as a function of the neutrino energy [37, 38]. Once a specific neutrino source is found and identified, for example from its energy spectrum or using information from its optical counterpart, it might be possible to select a specific flavor ratio at the source by applying suitable energy cuts to the data. However, note that, since the neutrino flux drops as the energy increases, we can expect less events from muon damped sources than from pion beam sources. In this work we will mainly focus on pion beam and on muon damped sources, as well as on neutrinos produced by photo-dissociation of heavy nuclei with a flavor composition  $(f_e, f_\mu, f_\tau) \simeq (1, 0, 0)$  at the source [39, 40] (“neutron beam source”). In some cases we will consider arbitrary flavor compositions at the source without significant tau neutrino production, as is expected from a diffuse flux coming from the superposition of pion beam and muon damped sources with different energy dependencies. For the identification of even more generalized sources including the possibility of tau neutrinos, see *e.g.* Ref. [41].

**Detector and observables.** On the detector side, flavor identification is the prerequisite to learn about neutrino properties. In a neutrino telescope such as IceCube, muon tracks can be most easily seen for  $E \gtrsim 100$  GeV. Electron and tau neutrinos will produce showers with a somewhat higher energy threshold,  $E \gtrsim 1$  TeV. In general, it is not possi-

ble to distinguish between electron and tau events close to the threshold, whereas at much higher energies one may be able to identify these flavors as well [42]. In particular, one may use the “double-bang” signature of  $\nu_\tau$  in a window  $5 \cdot 10^{14} \text{ eV} \lesssim E \lesssim 2 \cdot 10^{16} \text{ eV}$  to distinguish all flavors [43]. It is therefore plausible to assume that the ratios  $R \equiv \phi_\mu^{\text{det}} / (\phi_e^{\text{det}} + \phi_\tau^{\text{det}})$  (tracks/showers) and  $S \equiv \phi_e^{\text{det}} / \phi_\tau^{\text{det}}$  (electromagnetic/hadronic showers) can be used as observables, where  $\phi_\alpha^{\text{det}} = \hat{\phi}_{\alpha^+}^{\text{det}} + \hat{\phi}_{\alpha^-}^{\text{det}}$  is the neutrino (+) plus antineutrino (-) flux of flavor  $\nu_\alpha$  at the detector [26, 27]. As an additional observable, one may use  $T \equiv \hat{\phi}_{e^-}^{\text{det}} / \phi_\mu^{\text{det}}$  for the Glashow resonance process  $\bar{\nu}_e + e^- \rightarrow W^- \rightarrow \text{anything}$  at around 6.3 PeV [44, 25, 27] to distinguish between neutrinos and antineutrinos. Note that  $T$  is detectable only in a very narrow energy range, and that due to the difficulties in the identification of the double-bang the precision on  $S$  will be lower than the one on  $R$ . Moreover, for muon damped sources  $S$  will only be measurable in rare cases, because the typical energy window of this kind of source coincides only occasionally with the double-bang window.

This work is organized as follows. In Sec. 2 we describe the considered physics scenarios and we present a general classification of all possible decay schemes. In Sec. 3 we focus on normal mass hierarchy and discuss the possibility of identifying the decay scenario. The impact of the neutrino mass hierarchy and the possibility to establish it from astrophysical pion damped sources is discussed in Sec. 4. In Sec. 5 we extend our results to the case of unknown flavor compositions at the source, as is the case for certain diffuse fluxes. In Sec. 6 we study the Glashow resonance process as an additional observable, addressing the problem of the separation between neutrino and antineutrinos. In Sec. 7 we illustrate synergies with terrestrial neutrino oscillation experiments. Finally, in Sec. 8 we summarize our results and draw conclusions. Details of our statistics treatment can be found in Appendix A.

## 2. Considered physics scenarios

In this work we consider the most general combination between neutrino oscillations and arbitrary neutrino decay scenarios. This includes the conventional picture of oscillations among stable states as a limiting case. Concerning the oscillation part, we assume that oscillations take place only among the three known neutrino flavors, which means that sterile neutrino states – if they exist – do not mix with the active ones. As for the decay part, following the approach of Ref. [21] we assume that all unstable mass eigenstates have decayed between the source and the detector, *i.e.*, the decays are *complete*. Moreover, we neglect possible differences between neutrino and antineutrino decay rates, and we assume that if one polarity has completely decayed, the other one has as well. The decays products may be *visible* to the neutrino detector, *i.e.*, different active states, or *invisible* for the detector, such as sterile neutrinos, unparticle states, Majorons *etc.*. Since the decay is assumed to be complete and neutrino oscillations are completely averaged over astrophysical distances, the transition probabilities are independent of the neutrino energy. Therefore, in this study we do not take into account possible information on the energy spectrum, and only focus on total rates. In particular, we assume that the daughter neutrinos, if active states, fully contribute to the observed signal regardless of whether

Branchings ratios			\$1	\$2	\$3	\$4	\$5	\$6	\$7	\$8
			123	<del>123</del>	<del>123</del>	<del>123</del>	<del>123</del>	<del>123</del>	<del>123</del>	<del>123</del>
#1	LMH	-	$\begin{matrix} \textcircled{3} & \textcircled{2} \\ \textcircled{2} & \textcircled{1} \\ \textcircled{1} & \textcircled{3} \end{matrix}$	-	-	-	-	-	-	-
#2	<del>LMH</del>	$\text{Br}_{\text{H}\rightarrow\text{M}} = a, \text{Br}_{\text{H}\rightarrow\text{L}} = b$ $\text{Br}_{\text{H}\rightarrow\text{I}} = 1 - a - b$	$0 \leq a \leq 1$ $0 \leq b \leq 1 - a$	-	$\begin{matrix} \textcircled{3} \\ \textcircled{2} \\ \textcircled{1} \end{matrix}$	$\begin{matrix} \textcircled{2} \\ \textcircled{1} \\ \textcircled{3} \end{matrix}$	-	-	-	-
#3	<del>LMH</del>	$\text{Br}_{\text{M}\rightarrow\text{L}} = a, \text{Br}_{\text{M}\rightarrow\text{I}} = 1 - a$	$0 \leq a \leq 1$	-	-	$\begin{matrix} \textcircled{3} \\ \textcircled{2} \\ \textcircled{1} \end{matrix}$	$\begin{matrix} \textcircled{2} \\ \textcircled{1} \\ \textcircled{3} \end{matrix}$	-	-	-
#4	<del>LMH</del>	$\text{Br}_{\text{L}\rightarrow\text{I}} = 1$	-	-	$\begin{matrix} \textcircled{2} \\ \textcircled{1} \\ \textcircled{3} \end{matrix}$	-	$\begin{matrix} \textcircled{3} \\ \textcircled{2} \\ \textcircled{1} \end{matrix}$	-	-	-
#5	<del>LMH</del>	$\text{Br}_{\text{M}\rightarrow\text{I}} = 1$ $\text{Br}_{\text{L}\rightarrow\text{I}} = 1$	-	-	-	-	$\begin{matrix} \textcircled{3} \\ \textcircled{2} \\ \textcircled{1} \end{matrix}$	$\begin{matrix} \textcircled{2} \\ \textcircled{1} \\ \textcircled{3} \end{matrix}$	-	-
#6	<del>LMH</del>	$\text{Br}_{\text{H}\rightarrow\text{M}} = a, \text{Br}_{\text{H}\rightarrow\text{I}} = 1 - a$ $\text{Br}_{\text{L}\rightarrow\text{I}} = 1$	$0 \leq a \leq 1$	-	-	-	-	$\begin{matrix} \textcircled{3} \\ \textcircled{2} \\ \textcircled{1} \end{matrix}$	$\begin{matrix} \textcircled{2} \\ \textcircled{1} \\ \textcircled{3} \end{matrix}$	-
#7	<del>LMH</del>	$\text{Br}_{\text{H}\rightarrow\text{L}} = a, \text{Br}_{\text{H}\rightarrow\text{I}} = 1 - a$ $\text{Br}_{\text{M}\rightarrow\text{L}} = b, \text{Br}_{\text{M}\rightarrow\text{I}} = 1 - b$	$0 \leq a \leq 1$ $0 \leq b \leq 1$	-	-	-	$\begin{matrix} \textcircled{2} \\ \textcircled{1} \\ \textcircled{3} \end{matrix}$	-	$\begin{matrix} \textcircled{3} \\ \textcircled{2} \\ \textcircled{1} \end{matrix}$	-
#8	<del>LMH</del>	Not relevant, since no neutrinos observed		-	-	-	-	-	-	$\begin{matrix} \textcircled{3} & \textcircled{2} \\ \textcircled{2} & \textcircled{1} \\ \textcircled{1} & \textcircled{3} \end{matrix}$

**Table 1:** Classification of all the possible decay scenarios for complete decays, according to both LMH (rows) and 123 (columns) naming conventions. The tags “L”, “M”, “H” refer to the lightest, middle, heaviest active mass eigenstate, respectively, whereas “I” refers to an invisible state. The tags “1”, “2”, “3” refer to the  $\nu_1, \nu_2, \nu_3$  active mass eigenstates. A slash through the tag means that the corresponding state is unstable. The icons illustrate the correspondence between the two naming conventions according to the given mass hierarchy. The black and white disks correspond to stable and unstable mass eigenstates, respectively.

they are degraded in energy. Note that in some scenarios interference effects between oscillations and decay may occur if the source is coherent and the neutrinos decay while they are still oscillating [45, 46]; however, for the sake of simplicity we do not consider such cases or the corresponding corrections.

Let us now consider all possible decay scenarios in a systematic way. First of all, note that for kinematical reasons any mass eigenstate can only decay into lighter ones, which in turn may be stable or unstable. However, the assumption of *complete* decay allows to eliminate intermediate unstable states from every decay chain. For example, if the heaviest eigenstate decays into both the middle and the lightest state, and the middle state decays into the lightest state, finally everything will end up in the lightest state. This argumentation includes more complicated scenarios with arbitrary branching ratios, including active states decaying into invisible states which then decay back into active ones, as long as the initial states are active. It means that the transition probabilities can be

written in terms of the *effective* branching ratios  $\text{Br}_{i \rightarrow f}$  between the initial *unstable* active states  $\nu_i$  and the final *stable* active states  $\nu_f$ :

$$P_{\alpha\beta} = \sum_{f \text{ stable}} \left( |U_{\alpha f}|^2 + \sum_{i \text{ unstable}} |U_{\alpha i}|^2 \text{Br}_{i \rightarrow f} \right) |U_{\beta f}|^2. \quad (2.1)$$

Note that  $\sum_f \text{Br}_{i \rightarrow f} = 1$  only if there are no invisible final states, whereas in general  $\sum_f \text{Br}_{i \rightarrow f} \leq 1$ . Thus this formula also accounts for invisible final states.

As we have seen, any decay scenario is uniquely characterized by the stability of its active states. In general, there are  $2^3 = 8$  possibilities, since either active state may be stable or not. We list these possibilities in Table 1, together with the relevant parameters needed to completely describe each scenario. It is convenient to classify the various decay scenarios according to two different naming conventions:

**LMH classification.** This naming convention is illustrated in the *rows* of Table 1. The labels “L”, “M”, “H” refer to the lightest ( $\nu_L$ ), middle ( $\nu_M$ ), heaviest ( $\nu_H$ ) active mass eigenstate, respectively; a slash through the label (*e.g.*, “~~L~~”, “~~M~~”, “~~H~~”) means that the corresponding state is unstable. Different scenarios are denoted by  $\#n$ , with  $n = 1 \dots 8$ .

**123 classification.** This naming convention corresponds to the *columns* of Table 1. The labels “1”, “2”, “3” refer to the mass eigenstates  $\nu_1, \nu_2, \nu_3$  relevant for neutrino oscillations, irrespective of their mass ordering; as before, a slash through the label (*e.g.*, “~~1~~”, “~~2~~”, “~~3~~”) means that the corresponding state is unstable. Different scenarios are denoted by  $\$n$ , with  $n = 1 \dots 8$ .

The correspondence between these two classifications depends on the neutrino mass hierarchy; it is illustrated in Table 1. Specifically, for the normal hierarchy we simply have  $\#n = \$n$ , whereas for the inverted hierarchy we have  $\#1 = \$1$ ,  $\#2 = \$3$ ,  $\#3 = \$4$ ,  $\#4 = \$2$ ,  $\#5 = \$6$ ,  $\#6 = \$7$ ,  $\#7 = \$5$  and  $\#8 = \$8$ . Note that the branching ratios  $\text{Br}_{I \rightarrow F}$  are completely independent from the neutrino mass hierarchy when  $I$  and  $F$  are written in the LMH notation. Similarly, the matrix elements  $|U_{\alpha i}|^2$  and  $|U_{\alpha f}|^2$ , which appear in Eq. (2.1), are insensitive to the mass hierarchy when  $i$  and  $j$  are 123 tags. On the other hand, combinations of *both* mixing angles and branching ratios, such as the transition probabilities  $P_{\alpha\beta}$  in Eq. (2.1), do depend on the mass hierarchy. We will discuss the impact of the neutrino mass hierarchy in greater detail in Sec. 4.

The observables  $R$  and  $S$  defined in the previous section can be computed as

$$R = \frac{\sum_{\alpha} f_{\alpha} P_{\alpha\mu}}{\sum_{\alpha} f_{\alpha} (P_{\alpha e} + P_{\alpha\tau})}, \quad S = \frac{\sum_{\alpha} f_{\alpha} P_{\alpha e}}{\sum_{\alpha} f_{\alpha} P_{\alpha\tau}}. \quad (2.2)$$

Note that the overall flux normalization, which depends on the source luminosity, distance to the source, *etc.*, cancels in this definition. In addition, although the cross sections are not very well known at high energies, the valence quark contribution becomes negligible, and the dependence on the flavor becomes small [47, 48]. Therefore, we expect that the

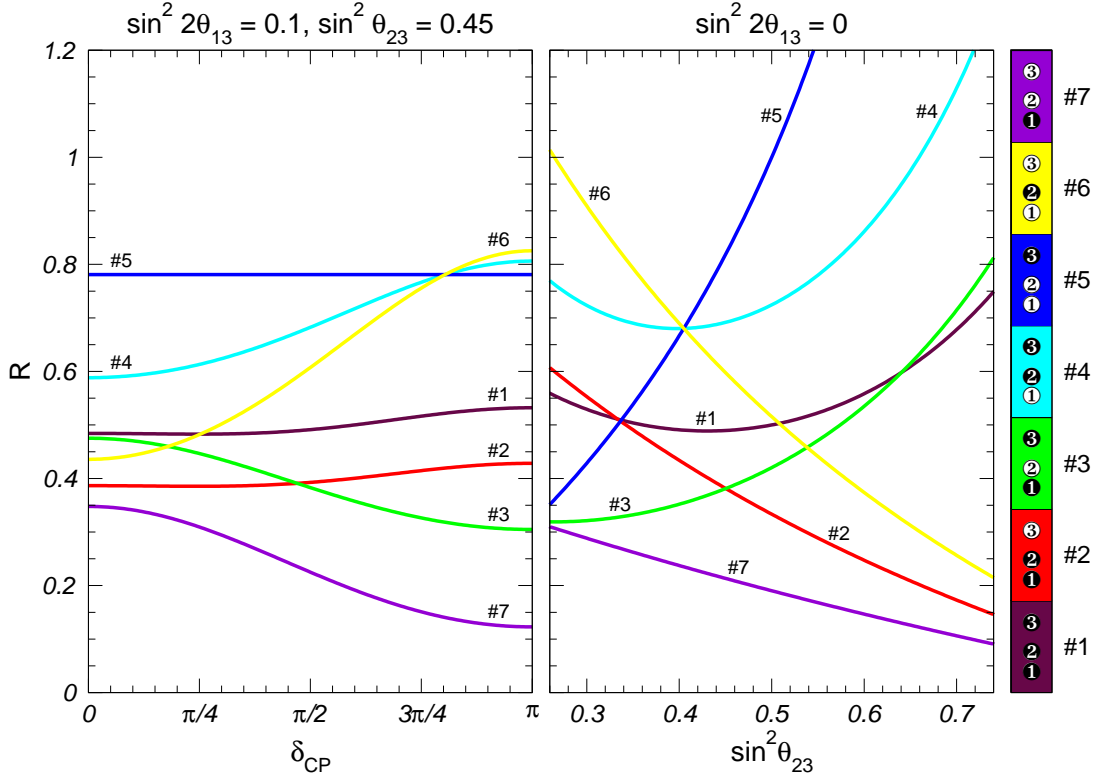


**Figure 1:** The observable  $R$  for a pion beam source as function of  $\delta_{\text{CP}}$  (left) and  $\sin^2 \theta_{23}$  (right) for the different scenarios in Table 1 (normal hierarchy assumed). We have chosen  $a = b = 0.5$  for scenarios #2 and #3.

uncorrelated cross section error among the different flavors are small, whereas the correlated cross section error cancels in Eq. (2.2).

An interesting special case is when there is only a *single* active stable neutrino mass eigenstate  $\nu_f$ . Substituting Eq. (2.1) in Eq. (2.2), it is straightforward to see that

$$R = \frac{|U_{\mu f}|^2}{|U_{ef}|^2 + |U_{\tau f}|^2} = \frac{|U_{\mu f}|^2}{1 - |U_{\mu f}|^2}, \quad S = \frac{|U_{ef}|^2}{|U_{\tau f}|^2} \quad (2.3)$$

since the probabilities factorize in source-dependent and detector-dependent parts. This means that in scenarios #6 and #7 the quantities  $R$  and  $S$  do not depend on the parameters  $a$  or  $b$  listed in Table 1, even if the probabilities do. In addition, Eq. (2.3) implies that there is no dependence on the  $f_\alpha$  characterizing the source, which means that the uncertainties on the source flavor composition are irrelevant for scenarios #5, #6 and #7.

To explicitly illustrate the kind of implications that the observation of an astrophysical neutrino source could have for neutrino phenomenology, we show in Fig. 1 the dependence of  $R$  on the parameters  $\delta_{\text{CP}}$  (for large  $\sin^2 2\theta_{13}$ ) and  $\sin^2 \theta_{23}$  (for small  $\sin^2 2\theta_{13}$ ). For definiteness we focus on the normal mass hierarchy and a pion beam source. As soon as a particular physics scenario is identified, a concrete measurement of  $R$  may considerably help in the determination of  $\delta_{\text{CP}}$  or  $\theta_{23}$ . In turn, if  $\delta_{\text{CP}}$ ,  $\theta_{13}$ , and  $\theta_{23}$  are constrained, we can use  $R$  to infer the decay scenario. For what concerns  $\delta_{\text{CP}}$ , scenarios #1, #2 and #5 are

obviously unfortunate, since there is little or no dependence on this parameter. However, if nature has implemented scenarios #3, #4, #6 or #7 astrophysical sources may provide very important information on  $\delta_{\text{CP}}$ . As for  $\theta_{23}$ , and in particular the octant determination, all scenarios may help, but scenarios #4, #5, and #6 are especially well suited. Note that there is some parameter dependence on the branching ratios in scenarios #2 and #3, while there is no dependence on the flavor composition at the source for scenarios #5, #6, and #7 as explained above. Such synergies between astrophysical and terrestrial experiments will be discussed in detail in the next sections.

Sometimes it may be useful to test additional assumptions coming from specific models. In addition to the general case, in this work we will consider the following special cases:

**Special case 1:** the lightest mass eigenstate  $\nu_L$  is stable. This constraint might be motivated by the observation of neutrinos from supernova 1987A. Only scenarios #1, #2, #3, and #7 are compatible with this assumption.

**Special case 2:** there are no invisible states. It follows that the lightest state must be stable, since it could only decay into a sterile state. Therefore, this case is a special realization of the previous one. In addition, the branching parameters become constrained: scenario #2 has now only one parameter ( $b = 1 - a$ ), and scenario #3 has no parameters at all ( $a = 1$ ).

### 3. Physics scenario identification

Let us now focus on the normal mass hierarchy (we will discuss the impact of the mass hierarchy in the next section) and let us assume that we can identify the source. Furthermore, we assume that information on both observables  $R$  (muon tracks to showers) and  $S$  (electromagnetic to hadronic showers) will be available. Under these hypotheses, the measurement of an astrophysical neutrino flux corresponds to a point in the  $(R, S)$  plane, with certain measurement errors.

In order to discuss to which extent one can in principle disentangle different physics scenarios, we show in Fig. 2 the 99% allowed regions corresponding to different decay scenarios. Specifically, we project the global  $\chi^2$  from present and future terrestrial experiments onto the  $(R, S)$  plane for each scenario, as the oscillation parameters and branching ratio parameters  $a$  and  $b$  (where applicable) are varied. The left and right columns correspond to muon damped and pion beam sources, respectively. In the upper panels we show 99% regions implied by the global analysis of present solar, atmospheric, reactor and accelerator neutrino data [49]. These experiments are further combined with the accurate measurement of  $\sin^2 2\theta_{13}$  expected after 3 years of Double Chooz data taking (1.5 of these with near detector), assuming that no signal ( $\sin^2 2\theta_{13} = 0$ , middle panels) or a large signal ( $\sin^2 2\theta_{13} = 0.1$ , lower panels) is observed.

Let us first of all focus on a pion beam source and current experiments, *i.e.*, the upper right panel in Fig. 2. Ignoring the uncertainties in the astrophysical measurement, scenarios #4, #5 and #7 are clearly separated from each other and from the rest. Although there is some overlap among the other scenarios, the physics can still be clearly identified in many



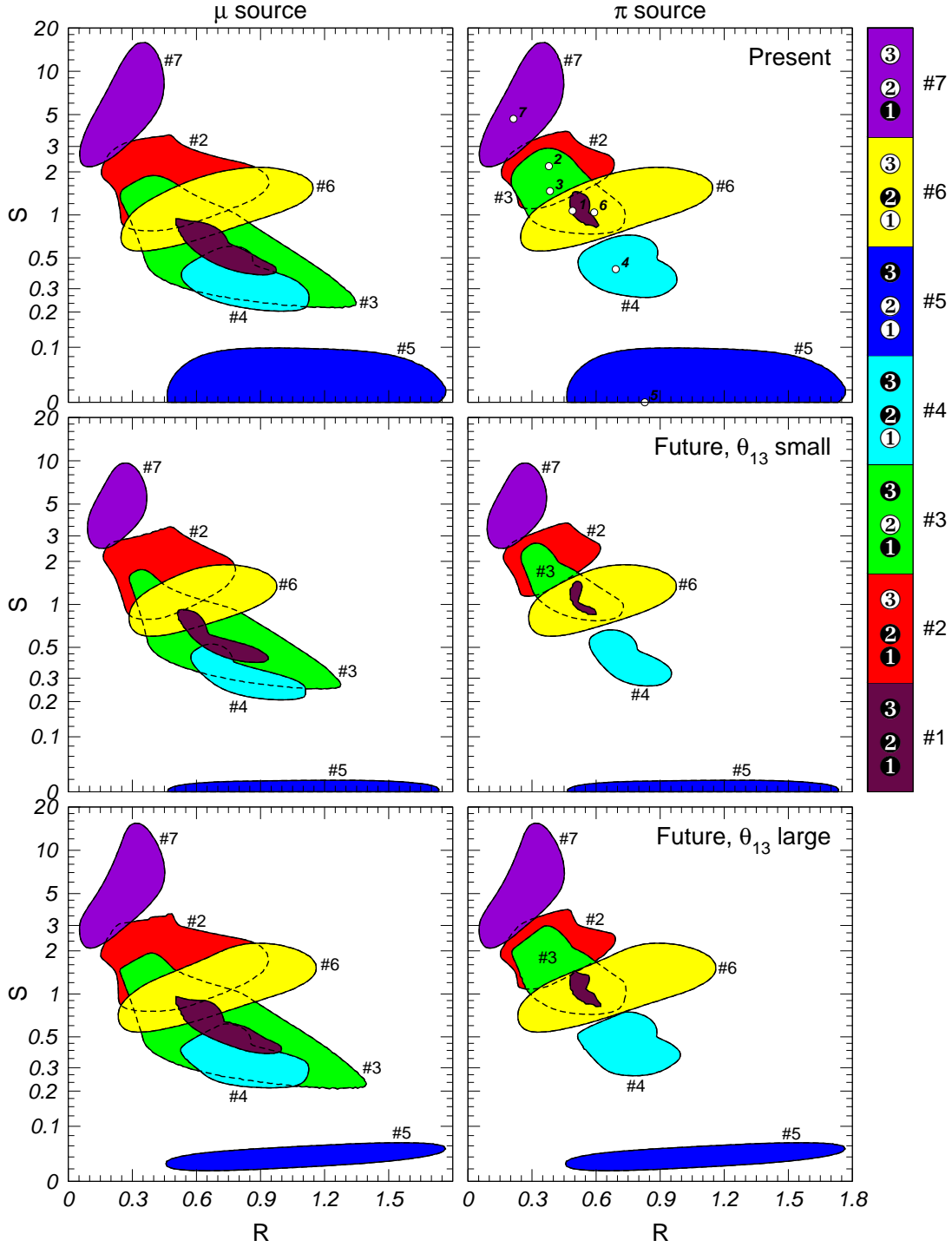


**Figure 2:** Allowed regions at 99% CL in the  $(R, S)$  plane corresponding to different decay scenarios, for a muon damped source (left panels) and a pion beam source (right panels). We assume a normal hierarchy. The upper panels correspond to the analysis of present data reported in Ref. [49]. The other panels show the impact of 3 years of Double Chooz data taking (1.5 with near detector), assuming no signal ( $\sin^2 2\theta_{13} = 0$ , middle panels) or a large signal ( $\sin^2 2\theta_{13} = 0.1$ , lower panels). The extra branching ratio parameters  $a$  and  $b$  have been varied as well, where applicable.

case. For example, a measurement  $(R, S) \simeq (1, 1.5)$  would uniquely determine scenario #6. Conversely, if one measures  $(R, S) \simeq (0.6, 1)$  there is some ambiguity among scenarios #1, #3, and #6, but scenarios #2, #4, #5, and #7 can still be excluded. Even if the observable  $S$  won't be available, in many cases one can clearly identify or exclude certain scenarios using only the projection onto the  $R$ -axis. For example, a measurement  $R = 1.5$  can only arise from scenario #5. The situation obviously improves if one includes in the analysis future terrestrial experiments such as Double Chooz, since the regions become somewhat smaller, although the qualitative picture does not change. Note, however, that the standard oscillation scenario #1 can never be uniquely established from astrophysical measurements, unless a further hypothesis on the stability of certain mass eigenstates are assumed a priori.

If we compare the pion beam source (upper right panel) with a muon damped source (upper left panel), we see that in general the allowed regions are much larger for the muon damped source. This means that the physics scenario identification becomes more difficult, but it also implies that the dependence on the individual parameters is stronger. Indeed it is well known that in the standard oscillation case (#1) the dependence of  $R$  and  $S$  on  $\sin^2 \theta_{23}$  and  $\delta_{\text{CP}}$  is considerably stronger for the muon damped source than for the pion beam source. It is also clear that the information from different sources is somewhat synergistic for what concerns the physics scenario identification. For example,  $(R, S) = (0.7, 0.5)$  single out scenario #4 for a pion beam source, whereas the scenario cannot be determined for a muon beam source. In turn,  $(R, S) = (1.2, 0.2)$  not only points towards scenario #3, but also uniquely identifies the source as muon damped, since for a pion beam source no region is present in this point of the parameter space. Moreover, note that scenarios #5, #6 and #7, which only have one stable active mass eigenstate, are independent of the source type, as we have pointed out in Eq. (2.3).

As the next step, let us simulate a realistic astrophysical measurement with concrete statistics. The details of our simple simulation are given in Appendix A. Note that we normalize the source luminosity to the number  $L$  of muon tracks which would be observed in the detector in the absence of neutrino decay (scenario #1) and for  $\sin^2 2\theta_{13} = 0$ . This means that we are properly using the same source luminosity for all the different scenarios. In general, a  $1\sigma$  error of order 10% might be expected for  $\mathcal{O}(100)$  events [26]. Since this error is much smaller than the typical size of the allowed regions shown in Fig. 2, we expect that our considerations hold as long as there are enough events. This statement is quantified in Table 2, which is based on the combination of present data with a simulated astrophysical measurement. The first three columns refer to the simulated scenario and the simulated  $R$  and  $S$  values, which are also plotted in the upper right panel of Fig. 2. The next seven columns give the  $\Delta\chi^2$  at which the corresponding decay scenario can be excluded, marginalized over all branching ratios and oscillation parameters. In the last two columns we marginalize also with respect to the fitted scenarios, giving the  $\Delta\chi^2$  and number of sigmas at which the simulated scenario can be established against *all* the others. The various blocks refer to different assumptions about statistics (muon tracks  $L$ ) and observables (either  $R$  alone or both  $R$  and  $S$  measured). This table clearly illustrates that even for low statistics (middle block) many scenarios can be excluded. For example, for

Simulated scenario			Fit scenario $\Delta\chi^2$								
No.	$R$	$S$	#1	#2	#3	#4	#5	#6	#7	Any	$\sigma$
<b>L=100, R+S measured:</b>											
#1	0.49	1.07	–	9.0	0.1	26.4	220.3	0.6	55.3	0.1	0.4
#2	0.38	2.19	21.0	–	0.4	73.1	432.1	20.0	20.6	0.4	0.6
#3	0.38	1.47	5.1	0.4	–	47.4	274.0	7.7	32.7	0.4	0.6
#4	0.69	0.41	20.7	53.3	17.9	–	43.7	15.4	115.7	15.4	3.9
#5	0.83	0.00	70.3	100.3	67.0	29.8	–	62.9	153.5	29.8	5.5
#6	0.59	1.04	1.1	8.4	0.9	12.8	106.2	–	48.2	0.9	1.0
#7	0.21	4.67	77.6	11.2	22.3	138.5	516.2	54.8	–	11.2	3.3
<b>L=10, R+S measured:</b>											
#1	0.49	1.07	–	1.2	0.0	4.8	36.2	0.1	13.0	0.0	0.2
#2	0.38	2.19	2.6	–	0.1	15.0	59.7	3.8	4.0	0.1	0.3
#3	0.38	1.47	0.6	0.1	–	8.2	41.7	1.2	6.2	0.1	0.3
#4	0.69	0.41	2.8	6.5	2.9	–	10.5	2.1	20.7	2.1	1.5
#5	0.83	0.00	7.7	10.9	7.8	3.3	–	7.0	20.6	3.3	1.8
#6	0.59	1.04	0.1	1.0	0.2	2.0	19.8	–	7.9	0.1	0.3
#7	0.21	4.67	8.7	1.2	3.2	23.4	67.7	10.4	–	1.2	1.1
<b>L=100, Only R measured:</b>											
#1	0.49	1.07	–	0.3	0.1	3.8	4.7	0.1	7.9	0.1	0.3
#2	0.38	2.19	3.7	–	0.0	13.6	11.6	1.4	2.4	0.0	0.0
#3	0.38	1.47	2.8	0.0	–	11.2	10.3	1.2	2.4	0.0	0.0
#4	0.69	0.41	4.8	4.2	2.9	–	0.3	0.3	18.4	0.3	0.5
#5	0.83	0.00	5.7	5.5	4.3	0.6	–	1.0	16.8	0.6	0.7
#6	0.59	1.04	1.1	1.5	0.9	0.2	1.3	–	10.5	0.2	0.5
#7	0.21	4.67	23.3	1.6	3.6	37.0	30.0	9.2	–	1.6	1.3

**Table 2:** Exclusion of different physics scenarios from present data plus astrophysical measurements, assuming normal mass hierarchy and a pion beam source. The first three columns refer to the simulated scenario and the simulated (benchmark)  $R$  and  $S$  values corresponding to the current best-fit values for the oscillation parameters and  $a = b = 0.5$  (where applicable). These points are marked in the upper right panel of Fig. 2. The next seven columns give the  $\Delta\chi^2$  at which the corresponding decay scenario can be excluded, marginalized over all branching ratios and oscillation parameters. In the last two columns we marginalize also with respect to the fitted “wrong” scenarios. The different groups assume different statistics (muon tracks  $L$ ) and either  $R$  and  $S$  as observables, or only  $R$  (*cf.*, Appendix A). The  $\chi^2$  from present solar, atmospheric, reactor, and accelerator data has been added [49].

simulated scenario #1 and only 10 muon tracks, scenarios #3 and #7 are ruled out at more than  $3\sigma$ . The same conclusion holds for higher statistics but no  $S$  measurement (lower block). In the high statistics case with both  $R$  and  $S$  measured (upper block) it is possible to uniquely establish scenarios #4, #5, and #7, excluding *all* the other ones.

An interesting and somewhat simpler issue is whether we can establish the stability of the lightest neutrino, *i.e.*, if special case 1 of Sec. 2 is realized. This corresponds to

the following questions: if the true scenario is one of #1, #2, #3, and #7 (in which the lightest neutrino is stable), can we rule out scenarios #4, #5, and #6? Conversely, if the real scenario is one of #4, #5, and #6 (in which the lightest neutrino is unstable), can we rule out scenarios #1, #2, #3, and #7? Focusing again on normal hierarchy and on a pion beam source, and assuming that both  $R$  and  $S$  can be measured, we can answer these questions by looking at the upper right panel of Fig. 2. Qualitatively, the perspectives to establish the stability of the lightest neutrino state depend on the true decay scenario, as follows:

**#1:** never (it is contained in #6);

**#2:** always (apart from a very small overlap with #6), if statistics is good enough;

**#3:** sometimes, if no overlap with #6 and there is enough statistics;

**#4:** always, if statistics is good enough;

**#5:** always, even with low statistics;

**#6:** sometimes, if no overlap with #2 and #3 and there is enough statistics;

**#7:** always, even with low statistics.

Therefore, the chances to determine whether the lightest state is stable or not over astrophysical distances are quite high.

#### 4. Neutrino mass hierarchy

As we have seen in Sec. 2, the neutrino mass hierarchy plays a crucial role in the correspondence between the two different naming conventions introduced in Table 1. Therefore, a detailed discussion of the main features of each scheme can help to understand the impact of the mass hierarchy on the scenario identification discussed so far. In the language of the LMH scheme, the branching ratios – and therefore the propagation from the astrophysical source to the neutrino detector – are completely independent of the hierarchy. On the other hand, the projection of the flavor states ( $\nu_e, \nu_\mu, \nu_\tau$ ) onto the mass eigenstates ( $\nu_L, \nu_M, \nu_H$ ) is different between normal and inverted hierarchy. This means that the production and detection processes, when described in terms of ( $\nu_L, \nu_M, \nu_H$ ), look different in the two hierarchies. For example, for the normal hierarchy,  $\nu_e$  is mostly  $\nu_L$ , but for the inverted hierarchy, it is mostly  $\nu_M$ . Therefore, the LMH convention provides a simpler description of the decay scenarios and is also more motivated from a theoretical (decay model) point of view, but it is not appropriate to describe oscillation phenomena. On the other hand, in the language of the 123 scheme, the relation between the flavor states ( $\nu_e, \nu_\mu, \nu_\tau$ ) and the mass states ( $\nu_1, \nu_2, \nu_3$ ) is the same for both hierarchies, but there is an asymmetry in the branching ratios created by kinematics, since heavier states can only decay into lighter ones. As an example, let us consider scenario \$2 ( $\nu_1$  and  $\nu_2$  stable,  $\nu_3$  unstable). For the normal hierarchy,  $\nu_3$  is the heaviest state and can decay into  $\nu_1$ , into  $\nu_2$ , or into

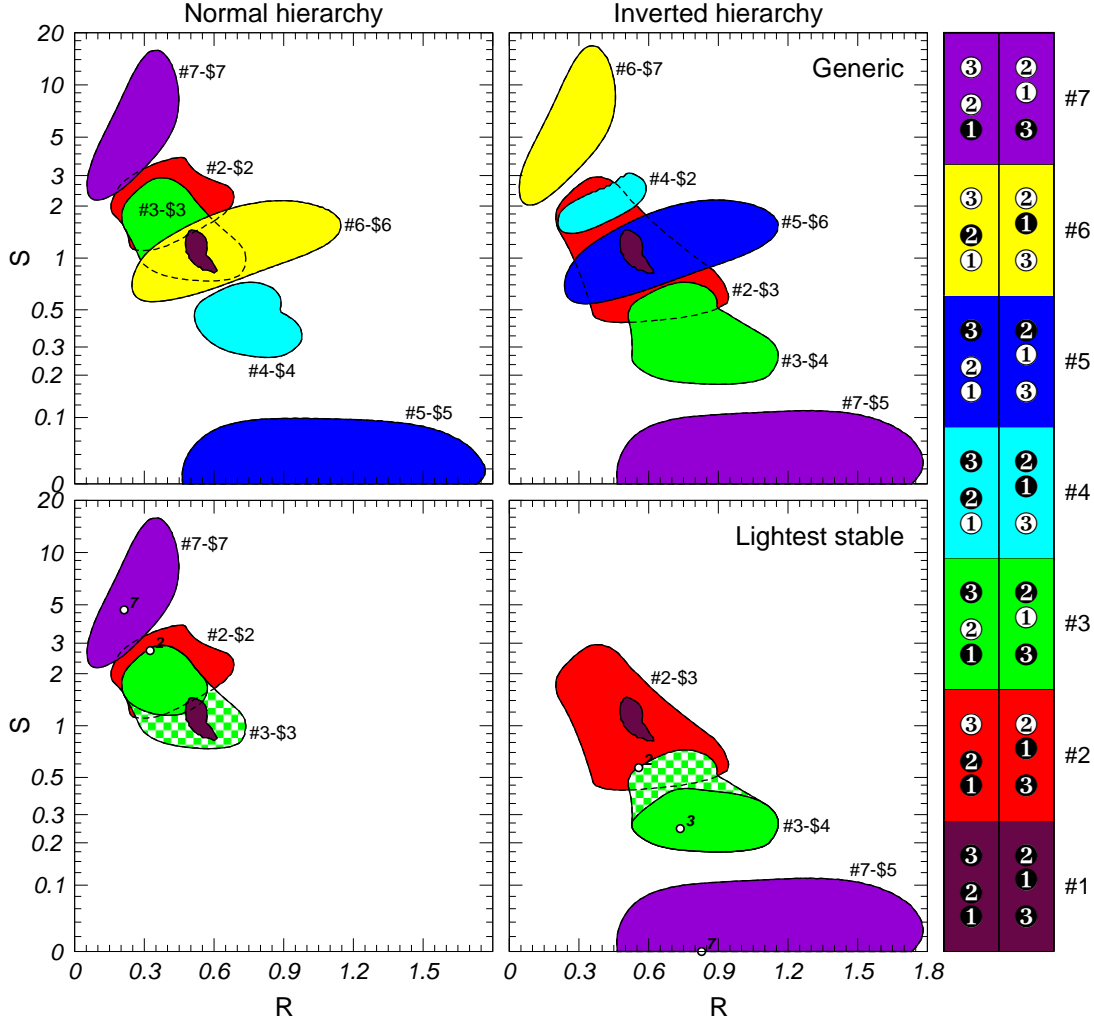


**Figure 3:** Allowed regions at 99% CL in the  $(R, S)$  plane corresponding to different decay scenarios, for the normal hierarchy (left panels) and the inverted hierarchy (right panels). We assume a pion beam source. The upper panels show the general case where all the scenario are allowed, while the lower panels correspond to the assumption that lightest mass eigenstate is stable (Special Case 1, see Sec. 2). If we further strengthen this restriction by imposing that there are no invisible states (Special Case 2), the patterned regions can be excluded as well.

invisible states, with a plethora of branching possibilities which are described in terms of two parameters (*cf.* Table 1). Conversely, for the inverted hierarchy,  $\nu_3$  is the lightest state and can only decay into invisible states without any further freedom. This implies that for scenario \$2 the branching possibilities for the inverted hierarchy are only a subset of those for the normal hierarchy, and hence the allowed region in the  $(R, S)$  plane for the inverted hierarchy is a subregion of the corresponding one for normal hierarchy. Similar analogies can be derived for scenarios \$3 and \$4. Note that scenario \$1 does not depend on the branching ratios and therefore there is no asymmetry between the normal and inverted hierarchy regions. The same happens for scenarios \$5, \$6 and \$7, since in this case the expressions for  $R$  and  $S$  are given by Eq. (2.3), which does not contain the branchings.

No.	Simulated scenario				Marginalized					
	$(a,b)$	Hier.	$R$	$S$	$\Delta\chi_0^2$	$\sigma_0$	$\Delta\chi_1^2$	$\sigma_1$	$\Delta\chi_2^2$	$\sigma_2$
#2	(0,1)	NH	0.33	2.72	2.6	1.6	3.6	1.9	3.6	1.9
#2	(0,1)	IH	0.56	0.57	4.2	2.0	10.4	3.2	12.0	3.5
#3	(1,-)	IH	0.74	0.25	3.8	1.9	51.5	7.2	63.1	7.9
#7	(-,-)	NH	0.21	4.67	0.0	0.2	13.4	3.7	13.4	3.7
#7	(-,-)	IH	0.83	0.00	0.1	0.2	67.0	8.2	70.4	8.4

**Table 3:** Identification of the neutrino mass hierarchy from astrophysical measurements only. The first four columns refer to the simulated scenario, hierarchy, and benchmark  $R$  and  $S$  values (marked in Fig. 3, lower row). The last six columns represent the overall  $\Delta\chi^2$  and  $\sigma$  for the wrong hierarchy exclusion marginalized over all physics scenarios. In these columns, we distinguish  $\Delta\chi_0^2$  and  $\sigma_0$  for no special assumptions,  $\Delta\chi_1^2$  and  $\sigma_1$  for special case 1 in Sec. 2 (lightest state stable), and  $\Delta\chi_2^2$  and  $\sigma_2$  for special case 2 in Sec. 2 (no invisible states). We assume  $L = 100$  muon tracks for this simulation of a pion beam source, and  $S$  and  $R$  to be measured. The  $\chi^2$  from present solar, atmospheric, reactor, and accelerator data has been added [49].

Note, however, that there are very small discrepancies between the two hierarchies due to the slight asymmetry introduced by present data [49].

Let us now discuss the the impact of the neutrino mass hierarchy on the physics scenario identification. In Fig. 3 we show the allowed regions in the  $(R, S)$  plane corresponding to different decay scenarios, for the normal hierarchy (left panels) and the inverted hierarchy (right panels). The colors represent the different scenarios in the LMH classification, but each region is explicitly labeled according to both schemes. From this figure we observe that the allowed domains corresponding to the same 123 scenario but to different hierarchies are quite similar, and one of the two is always a subregion of the other. Therefore, all the considerations presented in Sec. 3 about the identification of the decay scenario in the case of normal mass hierarchy are still qualitatively valid for the case of unknown hierarchy, provided that they are reformulated in the language of the 123 scheme. In other words, by measuring the  $(R, S)$  parameters we may be able to uniquely establish which of the  $(\nu_1, \nu_2, \nu_3)$  eigenstates are stable, but in order to convert this into a statement on the stability of  $(\nu_L, \nu_M, \nu_H)$  we need to know the mass hierarchy from an external source, such as long-baseline neutrino oscillation experiments (*cf.*, Sec. 7.3).

For what concerns the *mass hierarchy determination*, let us first consider the generic case with all possible decay scenarios, shown in the upper panels of Fig. 3. The fact that in a given 123 scenario the allowed region for one hierarchy is always a subregion of the one for the other hierarchy adds to the already mentioned problem of the degeneracy between different scenarios, and hence there is only a very limited portion of the parameter space where the hierarchy can be determined unambiguously by an astrophysical measurement. On the other hand, at the end of Sec. 2 we discussed a number of special cases reducing the number of possible decay scenarios and also restricting the corresponding parameter space. These special cases can be either motivated by specific decay models, or by phenomenological observations. For example, one may assume that the lightest mass eigenstate  $\nu_L$  is stable (special case 1). This constraint implies that only scenarios #1, #2, #3, and

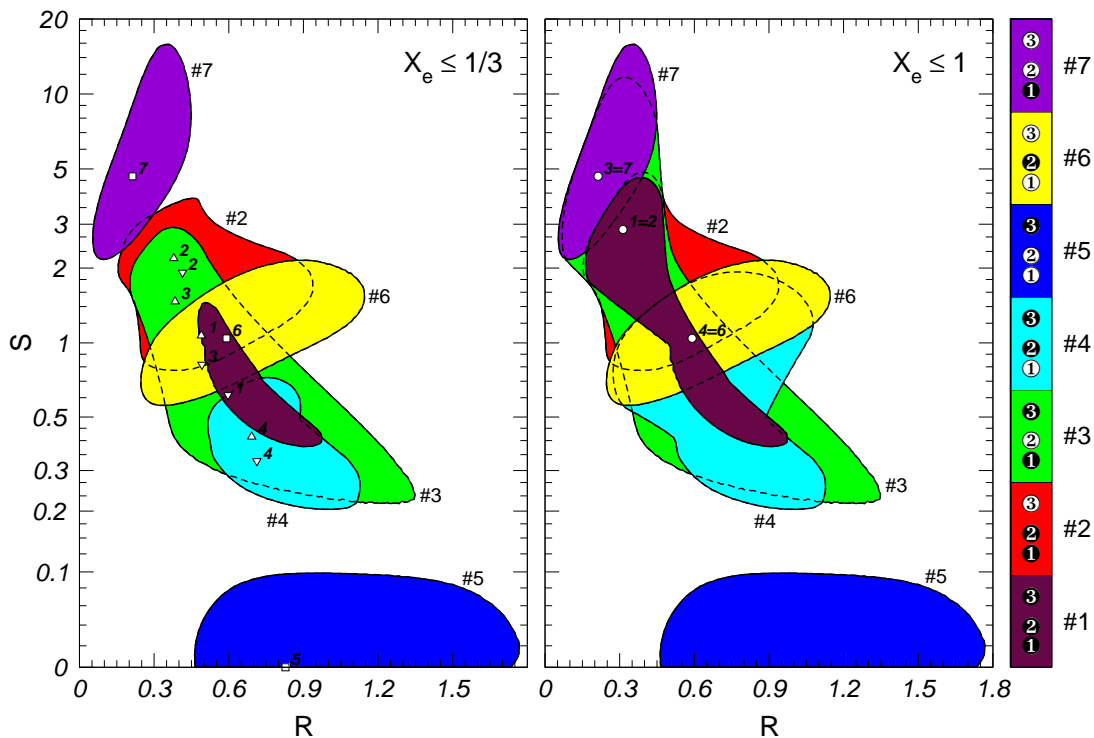


**Figure 4:** Allowed regions in the  $(R, S)$  plane for the normal hierarchy and an unknown source. The left panel corresponds to the electron fraction  $X_e$  marginalized over in the range  $0 \leq X_e \leq 1/3$ , while the right panel corresponds to it marginalized over the full range  $0 \leq X_e \leq 1$ . See main text for details.

#7 are remaining, as shown in the lower row of Fig. 3. If one further assumes that there are no invisible states (special case 2), then the allowed branching ratios become more restricted and the patterned regions disappear as well. Clearly, the mass hierarchy can be now easily determined: for example,  $R \gtrsim 1.2$  would imply scenario #7 and the inverted hierarchy. Note, however, that this interpretation of the experimental result is no longer purely phenomenological, and is intrinsically linked to the special assumption used.

We quantify this observation for several benchmark points in Table 3. The first four columns refer to the simulated scenario, hierarchy, and benchmark  $R$  and  $S$  values (marked in Fig. 3, lower panels). The last six columns represent the overall  $\Delta\chi^2$  and  $\sigma$  for the rejection of the wrong hierarchy, marginalized over all physics scenarios. Here we distinguish  $\Delta\chi_0^2$  and  $\sigma_0$  for no special assumptions,  $\Delta\chi_1^2$  and  $\sigma_1$  for special case 1 ( $\nu_L$  stable), and  $\Delta\chi_2^2$  and  $\sigma_2$  for special case 2 (no invisible states). As can be seen, in the general case at most a  $2\sigma$  mass hierarchy determination is possible, even for the relatively high luminosity considered here. On the other hand, in special case 1 the mass hierarchy can be easily measured in most of the discussed cases.

## 5. Generalized source or diffuse flux

Now what happens if we do not know anything about the source, such as if we have a

Simulated scenario			Fit scenario $\Delta\chi^2$								
No.	$R$	$S$	#1	#2	#3	#4	#5	#6	#7	Any	$\sigma$
<b>Simulated pion beam source, fit <math>0 \leq X_e \leq 1/3</math>: (<math>\Delta\Box</math>)</b>											
#1	0.49	1.07	–	1.0	0.0	26.4	220.3	0.6	55.3	0.0	0.1
#2	0.38	2.19	21.0	–	0.4	73.1	432.1	20.0	20.6	0.4	0.6
#3	0.38	1.47	5.1	0.2	–	47.4	274.0	7.7	32.7	0.2	0.4
#4	0.69	0.41	1.9	25.6	0.1	–	43.7	15.4	115.7	0.1	0.3
#5	0.83	0.00	40.2	74.4	27.5	24.0	–	62.9	153.5	24.0	4.9
#6	0.59	1.04	0.9	1.7	0.7	12.8	106.2	–	48.2	0.7	0.8
#7	0.21	4.67	77.6	11.1	22.3	138.5	516.2	54.8	–	11.1	3.3
<b>Simulated muon damped source, fit <math>0 \leq X_e \leq 1/3</math>: (<math>\nabla\Box</math>)</b>											
#1	0.60	0.61	–	13.8	0.0	4.0	96.1	5.3	99.5	0.0	0.1
#2	0.41	1.92	11.2	–	0.1	57.7	337.4	13.1	26.1	0.1	0.4
#3	0.49	0.82	0.2	4.1	–	13.2	125.9	0.4	62.0	0.2	0.5
#4	0.71	0.33	5.3	36.1	0.5	–	34.1	24.7	144.2	0.5	0.7
#5	0.83	0.00	51.6	92.9	35.2	31.1	–	80.2	192.1	31.1	5.6
#6	0.59	1.04	0.9	1.8	0.7	13.1	109.7	–	48.9	0.7	0.8
#7	0.21	4.67	60.8	8.8	18.5	116.2	401.5	49.1	–	8.8	3.0
<b>Simulated neutron beam source, fit <math>0 \leq X_e \leq 1</math>: (<math>\circ</math>)</b>											
#1=#2	0.31	2.86	–	–	0.0	35.5	740.0	35.5	10.5	0.0	0.0
#3=#7	0.21	4.67	14.0	14.0	–	72.9	810.9	72.8	–	14.0	3.7
#4=#6	0.59	1.04	0.8	1.6	0.6	–	95.3	–	45.9	0.6	0.8

**Table 4:** Same as Table 2 for different sources, and  $X_e$  marginalized in the indicated ranges. That means that here the source is assumed to be unknown to some degree, or one measures a diffuse flux (superposition of sources). Here  $L = 100$  and a measurement of  $R$  and  $S$  is assumed. The different (simulated) benchmark points are marked in Fig. 4. The  $\chi^2$  from present solar, atmospheric, reactor, and accelerator data has been added [49].

mixture of different sources, or even a diffuse flux? Can we still learn something about physics? Let us assume a flavor composition at source  $(X_e, 1 - X_e, 0)$ , *i.e.*,  $X_e = f_e$  is the electron (flavor) fraction, and there are no  $\nu_\tau$ 's produced. Such a flavor composition might be observed for a combination of different sources with different energy dependencies, or a diffuse flux. In these cases,  $X_e$  can be obtained as a (weighted) average of the different  $X_e^i$  from the different sources  $i$ . In the most general case, we have  $0 \leq X_e \leq 1$ , where  $X_e = 0$  corresponds to a  $\mu$ -damped source,  $X_e \simeq 1/3$  to a pion beam source, and  $X_e = 1$  to a source from neutron decays. Assuming that the neutrinos are only produced by pion decays (and partly subsequent muon decays) with an unknown energy dependence, we have  $0 \lesssim X_e \lesssim 0.35$  from Refs. [50, 34] including spectral effects. In general, any value of  $X_e$  is possible, but only one physics scenario will be realized if the decays are complete. Furthermore, let us assume, for the sake of simplicity, that we know the mass hierarchy from a different source.

We show in Fig. 4 the allowed regions for the observables  $R$  and  $S$  for the scenarios



from Table 1 for the normal hierarchy (99% CL). Let us first of all assume that we do not know anything about the source(s), *i.e.*,  $0 \leq X_e \leq 1$ . Therefore, we marginalize in the right panel of Fig. 4 over  $X_e$  in the full range  $0 \leq X_e \leq 1$ , which means that the regions span the whole range between muon damped and neutron beam source.<sup>1</sup> As the first observation, the scenario with only one final active stable state remains unchanged in consistency with Eq. (2.3). As a consequence, scenario #5 is still easy to identify. For the rest of the scenarios there is relatively strong overlap, and only in rare cases the scenarios might be identified. Nevertheless, many scenarios can still be excluded.

If we assume that only pion beam and muon damped sources (and mixtures of these) contribute, we find the result in the left panel of Fig. 4. Such a mixture might be measured for very limited energy resolution, unknown source parameters of a specific source, or a diffuse flux in a certain energy range. In this case, the result is qualitatively not extremely different from the previous discussion. For example, scenarios #5 and #7 are still relatively easy to identify. In addition, the conclusions from the previous chapters remain qualitatively unchanged. For a quantitative update, see Table 4, which is similar to Table 2, but for different sources, and  $X_e$  marginalized in the indicated ranges. That means that here the source is assumed to be unknown to some degree, or one measures a diffuse flux (superposition of sources). Here  $L = 100$ , and a simultaneous measurement of  $R$  and  $S$  is assumed. The different (simulated) benchmark points are marked in Fig. 4, where the first group corresponds to the triangles  $\triangle$  and squares  $\square$  the left panel (simulated  $X_e = 1/3$ ), the second group to the triangles  $\nabla$  and squares  $\square$  in the left panel (simulated  $X_e = 0$ ), and the third group to the circles  $\circ$  in the right panel (simulated  $X_e = 1$ ).<sup>2</sup> It is now very interesting to compare the first group in Table 4 to the first group in Table 2, which are only different by the marginalization over  $X_e$ . While in some cases the result does not change at all (such as for simulated scenario #1 and fit scenario #5), the sensitivity is in some cases completely destroyed (such as for simulated scenario #4 and fit scenario #3). This can be easily understood from Fig. 4, since the corresponding regions now overlap each other. Similar results are obtained for the simulated muon damped source in the middle row of Table 4. For the neutron beam source in the last row of Table 4 there is, however, a qualitative difference: Since the mass eigenstate  $\nu_3$  is initially not populated for  $X_e = 1$  because we assume a simulated  $\sin^2 2\theta_{13} = 0$  (and therefore  $U_{e3} = 0$ ; *cf.*, Eq. (2.1) and Eq. (2.2)), the stability of  $\nu_3$  is irrelevant, and models that differ only in that stability are physically equivalent. This means that the simulated models are paired, *i.e.*, #1=#2, #3=#7, #4=#6, #5=#8 (and this last case is irrelevant since nothing arrives at the detector).<sup>3</sup> From Table 4, it is quite interesting that in scenario #3=#7, any other qualitative case can be significantly excluded even if the only assumption on the source is that there are almost no  $\nu_\tau$ 's produced.

---

<sup>1</sup>For arbitrary marginalizations  $0 \leq X_e \leq X_e^{\max}$ , and arbitrary fixed  $X_e$ , see movies in Appendix B.

<sup>2</sup>Boxes are used if both points coincide, which is the case for all scenarios with only one stable mass eigenstate. In this case, the observables do not depend on the flavor composition at the source; *cf.*, Eq. (2.3).

<sup>3</sup>There can, however, be a difference in the fit  $\chi^2$  between two paired models, because we allow for  $\sin^2 2\theta_{13} > 0$  in the fit.

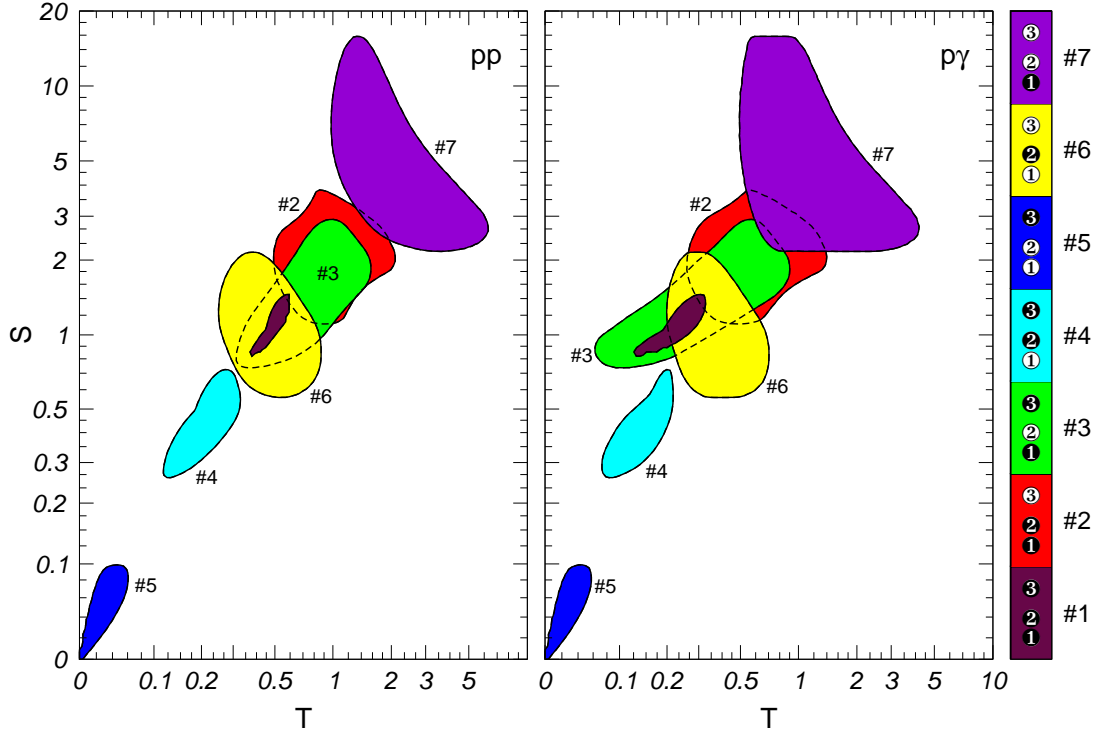


**Figure 5:** Allowed regions at 99% CL in the  $(T, S)$  plane, for a pion beam source and a normal hierarchy. The left panel corresponds to  $pp$  neutrino production, while the right panel corresponds to  $p\gamma$  production. In the legend, the black and white disks correspond to stable and unstable mass eigenstates, respectively.

## 6. Glashow resonance process as a third observable?

The Glashow resonance process  $\bar{\nu}_e + e^- \rightarrow W^- \rightarrow \text{anything}$  at around 6.3 PeV [44, 25] allows for the detection of electron antineutrinos only. Therefore, we define  $T = \hat{\phi}_{e^-}^{\text{det}} / \hat{\phi}_\mu^{\text{det}}$  as an additional observable. This is the only observable which is sensitive to the production of pions (and kaons) at the source by interactions of high energy protons with photons (“ $p\gamma$ ”) or protons (“ $pp$ ”) [51, 52, 53, 25]. In the  $p\gamma$  process, mainly  $\pi^+$  are produced through the  $\Delta$  resonance, which means that the flavor composition at the source is  $(\hat{f}_e, \hat{f}_\mu, \hat{f}_\tau | \hat{f}_{\bar{e}}, \hat{f}_{\bar{\mu}}, \hat{f}_{\bar{\tau}}) \simeq (\frac{1}{3}, \frac{1}{3}, 0 | 0, \frac{1}{3}, 0)$  (split up by neutrinos and antineutrinos with  $\sum \hat{f}_i = 1$ ). In the  $pp$  process, a nearly equal mix between  $\pi^+$  and  $\pi^-$  is produced, leading to  $(\hat{f}_e, \hat{f}_\mu, \hat{f}_\tau | \hat{f}_{\bar{e}}, \hat{f}_{\bar{\mu}}, \hat{f}_{\bar{\tau}}) \simeq (\frac{1}{6}, \frac{1}{3}, 0 | \frac{1}{6}, \frac{1}{3}, 0)$ . If the detector is CP-blind and there is no asymmetry between neutrinos and antineutrinos, we can sum the flavor compositions of neutrinos and antineutrinos at the source in order to obtain  $(f_e, f_\mu, f_\tau) = (\hat{f}_e + \hat{f}_{\bar{e}}, \hat{f}_\mu + \hat{f}_{\bar{\mu}}, \hat{f}_\tau + \hat{f}_{\bar{\tau}}) \simeq (\frac{1}{3}, \frac{2}{3}, 0)$  in both cases. Similarly, if the muons are damped at higher energies, we have  $(\hat{f}_e, \hat{f}_\mu, \hat{f}_\tau | \hat{f}_{\bar{e}}, \hat{f}_{\bar{\mu}}, \hat{f}_{\bar{\tau}}) \simeq (0, 1, 0 | 0, 0, 0)$  for  $p\gamma$ , and  $(\hat{f}_e, \hat{f}_\mu, \hat{f}_\tau | \hat{f}_{\bar{e}}, \hat{f}_{\bar{\mu}}, \hat{f}_{\bar{\tau}}) \simeq (0, \frac{1}{2}, 0 | 0, \frac{1}{2}, 0)$  for  $pp$ . In addition to the electron fraction  $X_e$  describing the fraction of electron neutrinos (and electron antineutrinos), one can introduce a photon fraction  $X_\gamma$  describing the fraction of neutrinos produced by  $p\gamma$  processes. In this case, the fraction  $1 - X_\gamma$  comes from  $pp$  interactions. If we assume that all electron neutrinos (antineutrinos)

come from antimuon (muon) decays, one can parameterize the source as

$$(\hat{f}_e, \hat{f}_\mu, \hat{f}_\tau | \hat{f}_{\bar{e}}, \hat{f}_{\bar{\mu}}, \hat{f}_{\bar{\tau}}) = \left( \frac{1 + X_\gamma}{2} X_e, \frac{1 + X_\gamma - X_e - 3X_\gamma X_e}{2}, 0 \left| \frac{1 - X_\gamma}{2} X_e, \frac{1 - X_\gamma - X_e + 3X_\gamma X_e}{2}, 0 \right. \right). \quad (6.1)$$

Conversely, the fraction of observed (useful) muon decays  $0 \leq \xi \leq 1$  is given by  $\xi = X_e/(1 - 2X_e)$ . Note that this parameterization can only describe the above decay chain, and is not useful for  $X_e > 1/3$ , such as for a neutron beam source.

We show in Fig. 5 the observables  $T$  and  $S$  for a pion beam source ( $X_e = 1/3$ ) and  $pp$  (left panel,  $X_\gamma = 0$ ) versus  $p\gamma$  interactions (right panel,  $X_\gamma = 1$ ).<sup>4</sup> Note that neither  $R$  nor  $S$  depend on  $X_\gamma$  since the neutrino and antineutrino rates are added. Since the regions do not collapse to thin curves, *i.e.*,  $T$  is a well-defined function  $T(S)$ , there is obviously additional useful information in  $T$ . However, in the  $pp$  case, the different scenarios cluster along the diagonal and overlap each other in the same fashion as for  $S$ . Therefore, for scenario identification,  $T$  may not provide much new information. For the  $p\gamma$  case, however, there is obviously new information. For example, if  $(T, S) = (0.1, 1)$  is measured, scenario #3 can be uniquely established, as well as the  $p\gamma$  source can be identified. If only  $R$  and  $S$  were used, it would be fully contained in clusters #2 and #6 (*cf.*, Fig. 2, upper right panel). Note that one can also establish the  $pp$  source in some cases. For example, if  $T \gtrsim 4$  is observed, scenario #7 together with a  $pp$  source has to be realized.

## 7. Synergies with terrestrial neutrino oscillation experiments

In this section we discuss the synergies with the terrestrial neutrino oscillation experiments. We focus on two decay scenarios, which are, in wide ranges of the parameters, relatively easy to identify: scenario \$5 (only  $\nu_3$  stable) and scenario \$7 (only  $\nu_1$  stable). Since in both cases there is only one stable mass eigenstate, the observables depend on the mixing matrix elements only (*cf.*, Eq. (2.3)). In particular, there is no dependence on the flavor composition at the source, branching ratios, and mass hierarchy. This means that there is also no mass hierarchy information from the astrophysical neutrino source(s). As discussed in Fig. 1,  $R$  varies strongly with  $\delta_{\text{CP}}$  in scenario \$7 (see also Ref. [32]), whereas  $R$  varies strongly with  $\theta_{23}$  in scenario \$5. Therefore, we use these two scenarios in combination with terrestrial measurements, and compare them to the standard oscillation result scenario (no decays) or the *same* luminosity of the source. As for the time scale, we choose the next generations of reactor and long-baseline experiments. Namely we use Double Chooz, MINOS, and NO $\nu$ A as examples. In addition, we assume that there are no decay effects observed in terrestrial experiments, *i.e.*, neutrino decay is visible only over astronomical distances. For details on the statistical simulation, see Appendix A.

### 7.1 Can Double Chooz plus neutrino telescope measure $\delta_{\text{CP}}$ ?

As in was pointed out in Refs. [26, 27], flavor ratio measurements might allow a measurement of  $\delta_{\text{CP}}$  already in combination with Double Chooz. However, for a pion beam source,

<sup>4</sup>For arbitrary  $X_\gamma$ , see movies in Appendix B.

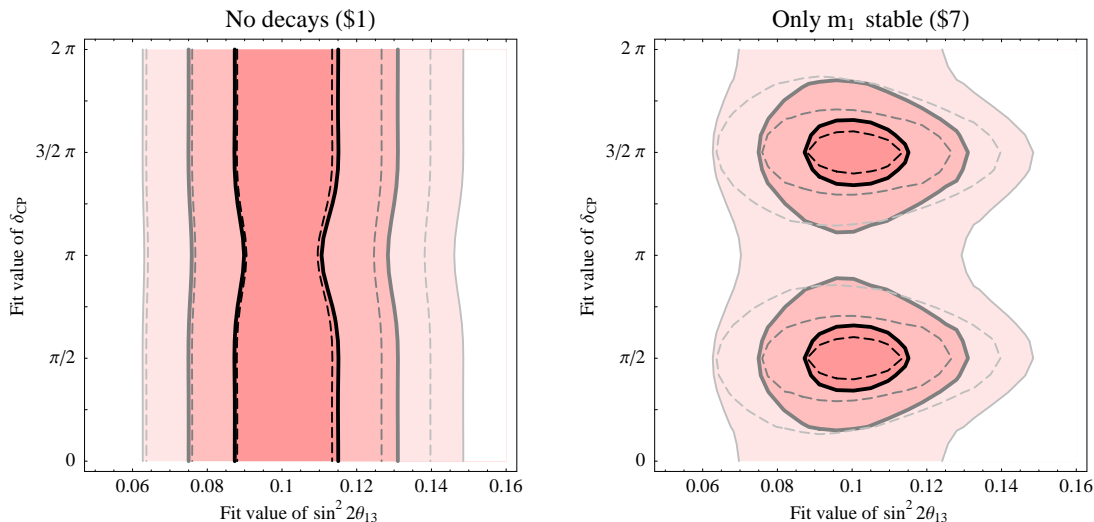


**Figure 6:** Comparison between physics scenarios \$1 (no decay, left column), and \$7 ( $\nu_1$  stable, right column), for Double Chooz plus an astrophysical source. Here a pion beam source  $L = 100$  tracks as normalized luminosity for both sources is assumed, *i.e.*, the left and right columns correspond to the same source luminosity. In addition, it is assumed that only  $R$  can be measured. The contours correspond to  $1\sigma$ ,  $2\sigma$ ,  $3\sigma$  (1 d.o.f.). The dashed curves are for fixing the other oscillation parameters. The current best-fit values and parameter errors are taken from Ref. [49]. The used simulated values are  $\sin^2 2\theta_{13} = 0.1$ ,  $\delta_{\text{CP}} = \pi/2$ , and a normal hierarchy.

which may be the most common one, the dependence of  $R$  and  $S$  on  $\delta_{\text{CP}}$  and the other oscillation parameters in the standard no-decay scenario is very moderate (*cf.*, Fig. 2). In this case, knowledge from different sources, high statistics, and the use of different observables is necessary to obtain useful information on  $\delta_{\text{CP}}$ . However, if neutrinos decay there can be a relatively strong dependence on  $\delta_{\text{CP}}$ , depending on the specific scenario [32]. We demonstrate this effect quantitatively for a three year Double Chooz measurement and a relatively large  $\sin^2 2\theta_{13}$  in Fig. 6. In this figure, the precision in  $\sin^2 2\theta_{13}$ - $\delta_{\text{CP}}$  is shown for maximal CP violation implemented by nature. For the astrophysical source, we only assume a pion beam source producing 100 muon tracks for the standard scenario, and we only measure the observable  $R$ . The left and right panels correspond to the same source luminosity. Obviously, if neutrinos are stable, there will be hardly any information on  $\delta_{\text{CP}}$ . However, if only  $\nu_1$  is stable, even a  $2\sigma$  CP violation measurement might be possible (if the uncertainties on the other oscillation parameters can be further reduced, even  $3\sigma$  – see dashed curves).

## 7.2 Octant determination terrestrial experiments plus neutrino telescope

The improvement of the octant measurement using astrophysical neutrinos was discussed in Ref. [26] for no decays and a combination of terrestrial experiments. Here we focus on a shorter time scale. We assume that we have information from Double Chooz and MINOS. From the left panel of Fig. 7 we can read off that there is no sensitivity to the octant in

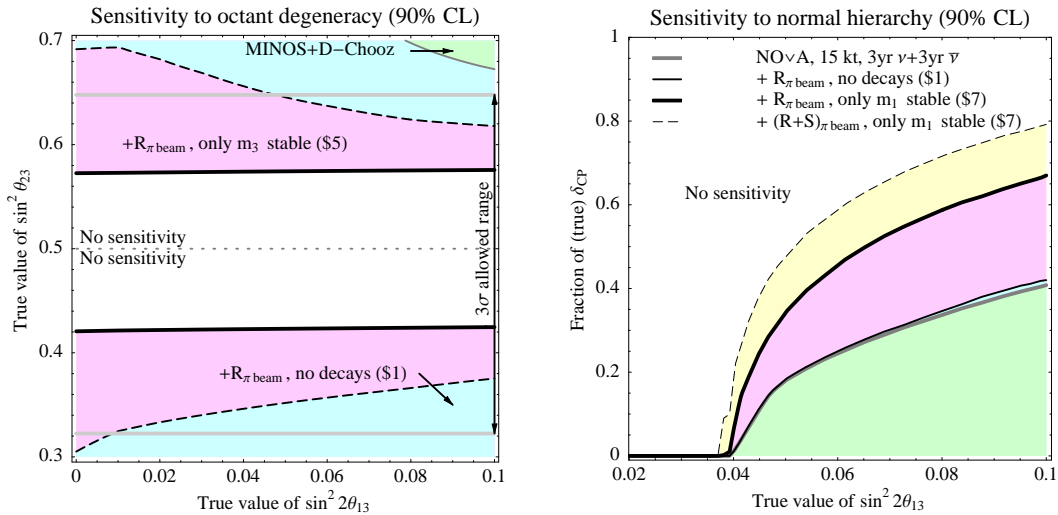


**Figure 7:** Left panel: Sensitivity to the octant degeneracy as a function of  $\sin^2 2\theta_{13}$  and  $\sin^2 \theta_{23}$ , 90% CL. The different curves represent MINOS plus Double Chooz alone, as well as these two experiments plus different astrophysical information for different physics scenarios. Right panel: Sensitivity to the normal mass hierarchy as a function of  $\sin^2 2\theta_{13}$  and  $\delta_{CP}$  (stacked to the “Fraction of  $\delta_{CP}$ ”), 90% CL. The different curves represent NO $\nu$ A alone, and NO $\nu$ A plus different astrophysical information for different physics scenarios. In both plots, sensitivity is given within the shaded regions,  $L = 100$  muon tracks were assumed for the flux normalization, and a normal hierarchy was simulated. The octant plot does not include the mixed (octant and sign) degeneracy. For details on the simulation, see Appendix A.

the  $3\sigma$  currently allowed  $\theta_{23}$  range (marked by the arrows). If  $R$  is measured for stable neutrinos (\$1) and for a pion beam source, the potential substantially improves compared to no astrophysical information, and includes wide region of the currently allowed range. However, if only  $\nu_3$  is stable (\$5), we can read off from Eq. (2.3) that

$$R = \frac{\sin^2 \theta_{23} \cos^2 \theta_{13}}{1 - \sin^2 \theta_{23} \cos^2 \theta_{13}} \simeq \tan^2 \theta_{23}. \quad (7.1)$$

This implies that  $\theta_{23}$  can be measured almost without parameter correlation by the neutrino telescope. In the left panel of Fig. 7 we show the excellent precision compared to scenario \$1 for the same source luminosity and observable, where the sensitivity mainly comes from the astrophysical source.

### 7.3 Mass hierarchy determination with NO $\nu$ A plus astrophysical

For terrestrial long-baseline experiments, the mass hierarchy degeneracy [54], which determines the mass hierarchy measurement, is, in general, located at a different value of  $\delta_{CP}$  than the original solution. In addition, it moves in the  $\delta_{CP}$  direction as a function of the true  $\sin^2 2\theta_{13}$  (*cf.*, Fig. 4 in Ref. [26] for NO $\nu$ A). Since astrophysical neutrino sources are sensitive to  $\cos \delta_{CP}$ , whereas first generation superbeams operated close to the oscillation

maximum are mainly sensitive to  $\sin \delta_{\text{CP}}$ , the knowledge from the astrophysical source can improve the mass hierarchy measurement at the terrestrial experiments [26]. This effect is largest in scenarios where the dependence of the observables on  $\delta_{\text{CP}}$  is strongest. We illustrate this behavior in the left panel of Fig. 7, where we compare our results for scenarios \$1 (no decays) and \$7 (only  $\nu_1$  stable) for a pion beam source. Note that, as explained before, there is no sensitivity at all to the mass hierarchy from the astrophysical source alone. As can be seen from this figure, there is almost no improvement for stable neutrinos (\$1), whereas if only  $\nu_1$  is stable (\$7), a measurement of  $R$  helps significantly, and additional information on  $S$  even more.

## 8. Summary and conclusions

In this study, we have discussed the identification of different decay and oscillation scenarios at neutrino telescopes. Furthermore, we have studied the measurement of the physics parameters within these scenarios by a neutrino telescope alone, and in combination with future terrestrial experiments. We have taken into account the present knowledge of the oscillation parameters from a global fit of current solar, atmospheric, reactor, and accelerator data, we have statistically quantified the information from the astrophysical sources, and we have performed a complete simulation of future terrestrial experiments. For the observables, we have mainly focused on the muon track to shower ratio and the electromagnetic to hadronic shower ratio, but we have also discussed the Glashow resonance process. We have performed a complete classification of effective decay scenarios and the corresponding branching ratios for complete decays, accounting also for possible invisible states. We have demonstrated that, depending on the physics scenario implemented by nature, the identification of the scenario can be unique or ambiguous. For example, if only  $\nu_1$  or  $\nu_3$  is stable (either of which can be the lightest depending on the hierarchy), the physics scenario can be easily identified. In the standard oscillation case, however, only specific scenarios can be excluded.

As far as the impact of the mass hierarchy is concerned, we have demonstrated that one may be able to establish which of the  $(\nu_1, \nu_2, \nu_3)$  mass eigenstates are stable, but not their mass ordering, which determines the branching ratios (since only heavier states can decay into lighter ones). For example, without external mass hierarchy measurement such as from superbeams, one can in principle determine whether  $\nu_1$  is stable or not, but not if  $\nu_1$  is the lightest or middle mass eigenstate. This implies that a generic mass hierarchy identification is only possible in very small corners of the parameter space. However, if one imposes some model-dependent constraints then the mass hierarchy can be easily determined in most cases from astrophysical neutrinos alone. One possible such constraint is the assumption that the lightest neutrino mass eigenstate is stable.

We have also studied the impact of flavor composition uncertainties at the source or the use of diffuse fluxes. For example, we have demonstrated that if no more than one active neutrino mass eigenstate is stable, there is no dependence of the observables on the flavor composition at the source. In order to study diffuse fluxes, we have marginalized the electron fraction at the source, which means that we have taken into account arbitrary

combinations of muon damped and pion beam sources. In this case, the physics scenario identification becomes quantitatively more difficult, but the qualitative conclusions still hold. Even if one allows for arbitrary production of  $\nu_e$  and  $\nu_\mu$  neutrinos at the source, some physics scenarios can still be established.

For what concerns the determination of the neutrino parameters in particular decay scenarios, we have chosen a number of examples in order to demonstrate the impact of an astrophysical measurement for future long-baseline and reactor experiments. For example, if a neutrino telescope measures the track to shower ratio from a pion beam source, then Double Chooz might be the first experiment to establish CP violation if  $\nu_1$  is the only stable state, whereas we have not found any CP violation sensitivity if all the neutrinos are stable. As another example, we have demonstrated that there is some sensitivity to the  $\theta_{23}$  octant if MINOS and Double Chooz are combined with astrophysical data even if all neutrino mass eigenstates are stable, but if only  $\nu_3$  is stable there will be direct octant sensitivity from the astrophysical source alone. We have also illustrated how the mass hierarchy sensitivity at NO $\nu$ A would be enhanced by an astrophysical neutrino measurement if only  $\nu_1$  is stable. For large  $\sin^2 2\theta_{13}$ , the fraction of  $\delta_{\text{CP}}$ , for which the hierarchy can be determined, could increase from 40% up to 80%. Note that this mass hierarchy determination is independent of any model-dependent assumptions on the decay scenarios.

We conclude that an observation of astrophysical neutrinos at a neutrino telescope would be an important test of the oscillation and decay neutrino properties.. While it is difficult to obtain information on the neutrino lifetime without a distance measurement of the source, complete decay scenarios can in many cases be easily identified even if one takes into account the current measurement precisions of the oscillation parameters and uncertainties of the flavor composition at the source. Especially if neutrinos decay, the combination with terrestrial neutrino experiments may lead to early and surprising results even for the standard oscillation parameter measurements. An important prerequisite for such conclusions will be the flavor identification in the detector. We therefore believe that establishing the flavor identification properties should be one of the key issues for any neutrino telescope experiment.

## Acknowledgments

We are grateful to Raj Gandhi for useful discussions. WW would like to thank the theory group at UAM for their hospitality during his visit. MM is supported by MEC through the Ramón y Cajal program and through the national project FPA2006-01105, by the Comunidad Autónoma de Madrid through the HEPHACOS project P-ESP-00346, and by the European Union through the ENTApP network of the ILIAS project RII3-CT-2004-506222. WW acknowledges support from the Emmy Noether program of Deutsche Forschungsgemeinschaft.

## A. Statistical method and simulation

A detailed description of our simulation of present solar, atmospheric, reactor and accel-

erator neutrino experiment can be found in Ref. [49], from which we also take the current best-fit values and allowed parameter ranges. For the MINOS simulation, we follow Ref. [55] with a total luminosity of  $5 \text{ yr} \times 3.7 \cdot 10^{20} \text{ pot/yr}$  and a 5.4 kt magnetized iron calorimeter [56] (the unit “pot/yr” refers to “protons on target per year”). For Double Chooz [57, 58], we use the simulation from Refs. [59, 60] with 1.5 years of data taking with far detector only, followed by 1.5 years with both detectors. For NO $\nu$ A, we use the simulation from Refs. [61, 26] updated to the numbers from Ref. [62] and a 15 kt detector mass. The future reactor and long-baseline experiments are simulated with the GLoBES software [63, 60].

We define an astrophysical  $\chi_{\text{astro}}^2$  to be added to the GLoBES software or to present experiments as

$$\chi_{\text{astro}}^2 = \min_{\xi} \left\{ 2 \sum_{i=1}^n \left[ T_i(\xi) - O_i + O_i \ln \frac{O_i}{T_i(\xi)} \right] + \left( \frac{\xi - 1}{\sigma_{\xi}} \right)^2 \right\}. \quad (\text{A.1})$$

Here  $T_i$  corresponds to the theoretical (fit) rate and  $O_i$  to the observed (true) rate. The index  $i$  runs over all event types (such as muon tracks, showers, double-bang, *etc.*). Here  $\xi$  is a source type-dependent unknown (free) flux normalization parameter to be marginalized over, and  $\sigma_{\xi}$  its error.

We consider two different cases for  $T$  and  $O$ . If only  $R$  is measured we set  $n = 2$  and

$$\begin{aligned} T_1 &= \xi N_{\mu}^{\text{fit}}, & T_2 &= \xi \left( N_e^{\text{fit}} + N_{\tau}^{\text{fit}} \right), \\ O_1 &= N_{\mu}^{\text{true}}, & O_2 &= N_e^{\text{true}} + N_{\tau}^{\text{true}}, \end{aligned} \quad (\text{A.2})$$

where  $N_{\beta}$  is the (total) number of events for flavor  $\nu_{\beta}$ . If both  $R$  and  $S$  are measured we set  $n = 3$  and

$$\begin{aligned} T_1 &= \xi N_{\mu}^{\text{fit}}, & T_2 &= \xi N_e^{\text{fit}}, & T_3 &= \xi N_{\tau}^{\text{fit}}, \\ O_1 &= N_{\mu}^{\text{true}}, & O_2 &= N_e^{\text{true}}, & O_3 &= N_{\tau}^{\text{true}}. \end{aligned} \quad (\text{A.3})$$

The event rate for the flavor  $\nu_{\beta}$  in the detector is given as

$$N_{\beta} = \phi \hat{\epsilon}_{\beta} \sum_{\alpha=1}^3 f_{\alpha} P_{\alpha\beta}^{(k)} \quad (\text{A.4})$$

where  $f_{\alpha}$  denotes the fraction of neutrinos produced as flavor  $\nu_{\alpha}$  at the source,  $\hat{\epsilon}_{\beta} \equiv \epsilon_{\beta}/\epsilon_{\mu}$  is a relative efficiency compared to the muon track detection efficiency,  $\phi$  corresponds to a normalized luminosity at the detector, and  $(k)$  refers to the decay scenario in Table 1 (the probability is described by Eq. (2.1)). In order to compare different physics scenarios for the same source flux, we normalize to a number of muon tracks  $L$  observed in the detector for the standard oscillation scenario #1 and  $\theta_{13} = 0$ , *i.e.*,

$$\phi = \frac{L}{\sum_{\alpha=1}^3 f_{\alpha} P_{\alpha\mu}^{(1)}}. \quad (\text{A.5})$$

This normalization does not depend on the physics scenario. Therefore, it allows to compare different physics scenarios for the same source flux, and one can identify the physics in



which one can most efficiently measure the target parameter. In addition, the number of observed muon tracks in the standard scenario is a quite intuitive one. For a flux close to the Waxmann-Bahcall bound, one may expect  $L = \mathcal{O}(100)$  muon tracks [27].

For the sake of simplicity, we assume that  $\hat{\epsilon}_e = \hat{\epsilon}_\tau = 1$ . In a more realistic simulation one would probably have  $\hat{\epsilon}_e, \hat{\epsilon}_\tau \ll 1$ , since the detector is sensitive to partially contained muon track events generated out of the fiducial volume, and the energy threshold for  $\mu$  events is lower [42]. Our assumption corresponds to choosing appropriate cuts such that  $\hat{\epsilon}_e \simeq \hat{\epsilon}_\tau \simeq 1$ , *i.e.*, muon tracks and the other event types are detected with similar efficiencies. For the case of  $S$ , that of course implies relatively low event rates. In addition, we assume a background-free environment. Backgrounds could be easily included in our treatment, but they strongly depend on the source type, energy range, *etc.*, whereas we want our simulation to be as much source-independent as possible. Finally, since we do not know the flux normalization, we use  $\sigma_\xi \rightarrow \infty$  in Eq. (A.1).

## B. Movies

A number of movies corresponding to Sec. 2, Sec. 5, and Sec. 6 can be found at Ref. [64].

The first type of movies uses  $X_e$  as a free parameter, *i.e.*, the time parameter, and corresponds to Fig. 2. The flavor composition at the source is assumed to be  $(f_e, f_\mu, f_\tau) = (X_e, 1 - X_e, 0)$ . Note that  $X_e = 0$  corresponds to a muon damped source,  $X_e = 1/3$  to a pion beam source, and  $X_e = 1$  to a neutron beam source. The movie shows the normal hierarchy (left) and the inverted hierarchy (right). Movie versions corresponding to all rows in Fig. 2 are available.

The second type of movies is similar to the first type, but  $X_e$  is marginalized over in the range  $0 \leq X_e \leq X_e^{\max}$ , and  $X_e^{\max}$  is the time frame parameter. This movie corresponds to Fig. 4, but movie versions corresponding to the different rows in Fig. 2 are available.

The third type of movies shows all observable pairs as a function of the photon fraction  $X_\gamma$  for a pion or muon damped source (versions for the different mass hierarchies are available as well). The photon fraction quantifies fraction of neutrinos is produced by  $p\gamma$  versus  $pp$  processes. For more details, see Sec. 6.

## References

- [1] **ANTARES** Collaboration, E. Aslanides *et al.*, *A deep sea telescope for high energy neutrinos*, [astro-ph/9907432](#).
- [2] **IceCube** Collaboration, J. Ahrens *et al.*, *Icecube: The next generation neutrino telescope at the south pole*, *Nucl. Phys. Proc. Suppl.* **118** (2003) 388–395, [[astro-ph/0209556](#)].
- [3] **NESTOR** Collaboration, S. E. Tzamarias, *Nestor: A deep-sea neutrino telescope*, *Nucl. Instrum. Meth.* **A502** (2003) 150–154.
- [4] **NEMO** Collaboration, P. Piattelli, *The neutrino mediterranean observatory project*, *Nucl. Phys. Proc. Suppl.* **143** (2005) 359–362.
- [5] S. Pakvasa, *Neutrino decays and neutrino telescopes*, [hep-ph/0305317](#).

- [6] **Particle Data Group** Collaboration, W. M. Yao *et al.*, *Review of particle physics*, *J. Phys.* **G33** (2006) 1–1232.
- [7] S. Pakvasa, *Neutrino Flavor Goniometry by High Energy Astrophysical Beams*, [arXiv:0803.1701 \[hep-ph\]](#).
- [8] G. G. Raffelt, *Neutrino radiative lifetime limits from the absence of solar gamma rays*, *Phys. Rev.* **D31** (1985) 3002–3004.
- [9] G. B. Gelmini and M. Roncadelli, *Left-handed neutrino mass scale and spontaneously broken lepton number*, *Phys. Lett.* **B99** (1981) 411.
- [10] Y. Chikashige, R. N. Mohapatra, and R. D. Peccei, *Spontaneously broken lepton number and cosmological constraints on the neutrino mass spectrum*, *Phys. Rev. Lett.* **45** (1980) 1926.
- [11] R. Tomas, H. Pas, and J. W. F. Valle, *Generalized bounds on Majoron neutrino couplings*, *Phys. Rev.* **D64** (2001) 095005, [[hep-ph/0103017](#)].
- [12] A. S. Joshipura, E. Masso, and S. Mohanty, *Constraints on decay plus oscillation solutions of the solar neutrino problem*, *Phys. Rev.* **D66** (2002) 113008, [[hep-ph/0203181](#)].
- [13] A. Bandyopadhyay, S. Choubey, and S. Goswami, *Neutrino decay confronts the SNO data*, *Phys. Lett.* **B555** (2003) 33–42, [[hep-ph/0204173](#)].
- [14] M. C. Gonzalez-Garcia and M. Maltoni, *Status of Oscillation plus Decay of Atmospheric and Long- Baseline Neutrinos*, [arXiv:0802.3699 \[hep-ph\]](#).
- [15] S.-L. Chen, X.-G. He, and H.-C. Tsai, *Constraints on unparticle interactions from invisible decays of  $z$ , quarkonia and neutrinos*, [arXiv:0707.0187 \[hep-ph\]](#).
- [16] S. Zhou, *Neutrino decays and neutrino electron elastic scattering in unparticle physics*, [arXiv:0706.0302 \[hep-ph\]](#).
- [17] X.-Q. Li, Y. Liu, and Z.-T. Wei, *Neutrino decay as a possible interpretation to the miniboone observation with unparticle scenario*, [arXiv:0707.2285 \[hep-ph\]](#).
- [18] D. Majumdar, *Unparticle decay of neutrinos and it's effect on ultra high energy neutrinos*, [arXiv:0708.3485 \[hep-ph\]](#).
- [19] R. L. Awasthi and S. Choubey, *Confusing Sterile Neutrinos with Deviation from Tribimaximal Mixing at Neutrino Telescopes*, *Phys. Rev.* **D76** (2007) 113002, [[arXiv:0706.0399 \[hep-ph\]](#)].
- [20] C. Quigg, *Cosmic Neutrinos*, [arXiv:0802.0013 \[hep-ph\]](#).
- [21] J. F. Beacom, N. F. Bell, D. Hooper, S. Pakvasa, and T. J. Weiler, *Decay of high-energy astrophysical neutrinos*, *Phys. Rev. Lett.* **90** (2003) 181301, [[hep-ph/0211305](#)].
- [22] Y. Farzan and A. Y. Smirnov, *Leptonic unitarity triangle and  $cp$ -violation*, *Phys. Rev.* **D65** (2002) 113001, [[hep-ph/0201105](#)].
- [23] P. D. Serpico and M. Kachelriess, *Measuring the  $13$ -mixing angle and the  $cp$  phase with neutrino telescopes*, *Phys. Rev. Lett.* **94** (2005) 211102, [[hep-ph/0502088](#)].
- [24] P. D. Serpico, *Probing the  $2$ - $3$  leptonic mixing at high-energy neutrino telescopes*, *Phys. Rev.* **D73** (2006) 047301, [[hep-ph/0511313](#)].
- [25] P. Bhattacharjee and N. Gupta, *Probing neutrino mixing angles with ultrahigh energy neutrino telescopes*, [hep-ph/0501191](#).

- [26] W. Winter, *How astrophysical neutrino sources could be used for early measurements of neutrino mass hierarchy and leptonic  $cp$  phase*, *Phys. Rev.* **D74** (2006) 033015, [[hep-ph/0604191](#)].
- [27] K. Blum, Y. Nir, and E. Waxman, *Probing  $cp$  violation in neutrino oscillations with neutrino telescopes*, [arXiv:0706.2070](#) [[hep-ph](#)].
- [28] W. Rodejohann, *Neutrino mixing and neutrino telescopes*, *JCAP* **0701** (2007) 029, [[hep-ph/0612047](#)].
- [29] Z.-z. Xing, *Neutrino telescopes as a probe of broken mu tau symmetry*, *Phys. Rev.* **D74** (2006) 013009, [[hep-ph/0605219](#)].
- [30] G.-R. Hwang and K. Siyeon, *Neutrino telescopes and the degeneracy problem*, [arXiv:0711.3122](#) [[hep-ph](#)].
- [31] S. Choubey, V. Niro, and W. Rodejohann, *On Probing  $\theta_{23}$  in Neutrino Telescopes*, [arXiv:0803.0423](#) [[hep-ph](#)].
- [32] J. F. Beacom, N. F. Bell, D. Hooper, S. Pakvasa, and T. J. Weiler, *Sensitivity to  $\theta_{13}$  and  $\delta$  in the decaying astrophysical neutrino scenario*, *Phys. Rev.* **D69** (2004) 017303, [[hep-ph/0309267](#)].
- [33] D. Meloni and T. Ohlsson, *Neutrino flux ratios at neutrino telescopes: The role of uncertainties of neutrino mixing parameters and applications to neutrino decay*, *Phys. Rev.* **D75** (2007) 125017, [[hep-ph/0612279](#)].
- [34] S. Pakvasa, W. Rodejohann, and T. J. Weiler, *Flavor ratios of astrophysical neutrinos: Implications for precision measurements*, [arXiv:0711.4517](#) [[hep-ph](#)].
- [35] A. Loeb and E. Waxman, *A guaranteed flux of extra-galactic high-energy neutrinos*, [astro-ph/0601695](#).
- [36] T. Kashti and E. Waxman, *Flavoring astrophysical neutrinos: Flavor ratios depend on energy*, *Phys. Rev. Lett.* **95** (2005) 181101, [[astro-ph/0507599](#)].
- [37] M. Kachelriess and R. Tomas, *High energy neutrino yields from astrophysical sources. i: Weakly magnetized sources*, *Phys. Rev.* **D74** (2006) 063009, [[astro-ph/0606406](#)].
- [38] M. Kachelriess, S. Ostapchenko, and R. Tomas, *High energy neutrino yields from astrophysical sources ii: Magnetized sources*, [arXiv:0708.3047](#) [[astro-ph](#)].
- [39] L. A. Anchordoqui, H. Goldberg, F. Halzen, and T. J. Weiler, *Galactic point sources of  $\tau$  antineutrinos*, *Phys. Lett.* **B593** (2004) 42, [[astro-ph/0311002](#)].
- [40] D. Hooper, D. Morgan, and E. Winstanley, *Probing quantum decoherence with high-energy neutrinos*, *Phys. Lett.* **B609** (2005) 206–211, [[hep-ph/0410094](#)].
- [41] Z.-Z. Xing and S. Zhou, *Towards determination of the initial flavor composition of ultrahigh-energy neutrino fluxes with neutrino telescopes*, *Phys. Rev.* **D74** (2006) 013010, [[astro-ph/0603781](#)].
- [42] J. F. Beacom, N. F. Bell, D. Hooper, S. Pakvasa, and T. J. Weiler, *Measuring flavor ratios of high-energy astrophysical neutrinos*, *Phys. Rev.* **D68** (2003) 093005, [[hep-ph/0307025](#)].  
Erratum-ibid.D72, 019901 (2005).
- [43] J. G. Learned and S. Pakvasa, *Detecting tau-neutrino oscillations at  $pev$  energies*, *Astropart. Phys.* **3** (1995) 267–274, [[hep-ph/9405296](#)].

- [44] L. A. Anchordoqui, H. Goldberg, F. Halzen, and T. J. Weiler, *Neutrinos as a diagnostic of high energy astrophysical processes*, *Phys. Lett.* **B621** (2005) 18–21, [[hep-ph/0410003](#)].
- [45] M. Lindner, T. Ohlsson, and W. Winter, *A combined treatment of neutrino decay and neutrino oscillations*, *Nucl. Phys.* **B607** (2001) 326–354, [[hep-ph/0103170](#)].
- [46] M. Lindner, T. Ohlsson, and W. Winter, *Decays of supernova neutrinos*, *Nucl. Phys.* **B622** (2002) 429–456, [[astro-ph/0105309](#)].
- [47] R. Gandhi, C. Quigg, M. H. Reno, and I. Sarcevic, *Ultra-high-energy neutrino interactions*, *Astropart. Phys.* **5** (1996) 81–110, [[hep-ph/9512364](#)].
- [48] R. Gandhi, C. Quigg, M. H. Reno, and I. Sarcevic, *Neutrino interactions at ultrahigh energies*, *Phys. Rev.* **D58** (1998) 093009, [[hep-ph/9807264](#)].
- [49] M. C. Gonzalez-Garcia and M. Maltoni, *Phenomenology with massive neutrinos*, [arXiv:0704.1800](#) [[hep-ph](#)].
- [50] P. Lipari, M. Lusignoli, and D. Meloni, *Flavor composition and energy spectrum of astrophysical neutrinos*, *Phys. Rev.* **D75** (2007) 123005, [[arXiv:0704.0718](#) [[astro-ph](#)]].
- [51] F. W. Stecker, *Effect of photomeson production by the universal radiation field on high-energy cosmic rays*, *Phys. Rev. Lett.* **21** (1968) 1016–1018.
- [52] V. L. Ginzburg, V. A. Dogiel, V. S. Berezhinsky, S. V. Bulanov, and V. S. Ptuskin, *Astrophysics of cosmic rays*, . Amsterdam, Netherlands: North-Holland (1990) 534 p.
- [53] T. K. Gaisser, F. Halzen, and T. Stanev, *Particle astrophysics with high-energy neutrinos*, *Phys. Rept.* **258** (1995) 173–236, [[hep-ph/9410384](#)].
- [54] H. Minakata and H. Nunokawa, *Exploring neutrino mixing with low energy superbeams*, *JHEP* **10** (2001) 001, [<http://arXiv.org/abs/hep-ph/0108085>].
- [55] P. Huber, M. Lindner, M. Rolinec, T. Schwetz, and W. Winter, *Prospects of accelerator and reactor neutrino oscillation experiments for the coming ten years*, *Phys. Rev.* **D70** (2004) 073014, [[hep-ph/0403068](#)].
- [56] **MINOS** Collaboration, E. Ables *et al.*, *P-875: A long baseline neutrino oscillation experiment at fermilab*, . FERMILAB-PROPOSAL-P-875.
- [57] F. Ardellier *et al.*, *Letter of intent for double-chooz: A search for the mixing angle  $\theta_{13}$* , [hep-ex/0405032](#).
- [58] **Double Chooz** Collaboration, F. Ardellier *et al.*, *Double chooz: A search for the neutrino mixing angle  $\theta_{13}$* , [hep-ex/0606025](#).
- [59] P. Huber, J. Kopp, M. Lindner, M. Rolinec, and W. Winter, *From double chooz to triple chooz: Neutrino physics at the chooz reactor complex*, *JHEP* **05** (2006) 072, [[hep-ph/0601266](#)].
- [60] P. Huber, J. Kopp, M. Lindner, M. Rolinec, and W. Winter, *New features in the simulation of neutrino oscillation experiments with globes 3.0*, *Comput. Phys. Commun.* **177** (2007) 432–438, [[hep-ph/0701187](#)].
- [61] P. Huber, M. Lindner, and W. Winter, *Synergies between the first-generation jhf-sk and numi superbeam experiments*, *Nucl. Phys.* **B654** (2003) 3–29, [[hep-ph/0211300](#)].
- [62] **NOvA** Collaboration, D. S. Ayres *et al.*, *Nova proposal to build a 30-kiloton off-axis detector to study neutrino oscillations in the fermilab numi beamline*, [hep-ex/0503053](#).

- [63] P. Huber, M. Lindner, and W. Winter, *Simulation of long-baseline neutrino oscillation experiments with globes*, *Comput. Phys. Commun.* **167** (2005) 195, [hep-ph/0407333].  
<http://www.mpi-hd.mpg.de/lin/globes/>.
- [64] M. Maltoni and W. Winter, “Movie webpage.”  
<http://theorie.physik.uni-wuerzburg.de/~winter/Resources/AstroMovies.html>.